PPPL-3140- Preprint Date: November1995, UC-420, 426

High Frequency Core Localized Modes in Neutral Beam Heated Plasmas on TFTR

R. Nazikian, Z. Chang, E.D. Fredrickson, S.H. Batha, R. Bell, R. Budny, C.E. Bush, C.Z. Cheng, A. Janos, F. Levinton, J. Manickam, E. Mazzucato, H.K. Park, G. Rewoldt, S. Sabbagh, E.J. Synakowski, W. Tang, G. Taylor, L.E. Zakharov

Princeton Plasma Physics Laboratory
Princeton University, P.O . Box 451, Princeton NJ 08540-0451

Abstract

A band of high frequency modes in the range 50-150 kHz with intermediate toroidal mode numbers $4<n<10$ are commonly observed in the core of supershot plasmas on TFTR. Two distinct varieties of MHD modes are identified corresponding to a flute-like mode predominantly appearing around the $q = 1$ surface and an outward ballooning mode for $q > 1$. The flute-like modes have nearly equal amplitude on the high field and low field side of the magnetic axis and are mostly observed in moderate performance supershot plasmas with $\tau_E < 2\tau_L$, while the ballooning-like modes have enhanced amplitude on the low field side of the magnetic axis and tend to appear in higher performance supershot plasmas with $\tau_E > 2\tau_L$, where τ_L is the equivalent L-mode confinement time. The modes propagate in the ion diamagnetic drift direction and are highly localized with radial widths $\Delta r \sim 5-10$ cm, fluctuation levels $\tilde{n}/n$, $\tilde{T}_e/T_e < 0.01$, and radial displacements $\xi_r \sim 0.1$ cm. Unlike the toroidally localized high-n activity observed just prior to major and minor disruptions on TFTR [1], these modes are typically much weaker more benign, and may be indicative of kinetic ballooning modes destabilized by resonant circulating neutral beam ions.

Introduction

The investigation of high-n MHD activity is of continuing importance in fusion research given the general view that such activity limits the maximum achievable plasma pressure in a tokamak reactor [2,3]. Theoretical investigations into MHDphasis on the ballooning modes which are considered one of the primary candidates for limiting the performance of magnetic confinement systems at high β ($\equiv$plasma pressure/magnetic pressure) [4-7]. Much of the work in recent years has focused the importance of non-ideal effects on mode stability such as resonant and non-resonant contributions of thermal and energetic particles [8-12]. The emerging picture from the kinetic analysis is that ballooning modes may be driven unstable by resonant particles below the ideal MHD threshold, but that unlike the ideal instabilities, the kinetic ballooning modes (KBMs) should exhibit significantly lower growth rates and lower saturated amplitudes. Their importance is that they may enhance the local thermal and particle transport, thereby limiting the maximum achievable β, and more importantly they may resonate with energetic fusion products, thereby limiting the alpha heating efficiency in a fusion reactor. The experimental challenge is to determine whether high-n MHD activity is at all prevalent in existing large scale devices during strong auxiliary heating, and if so then to determine whether these modes have a significant effect on plasma confinement. Given the substantial effort invested in the theoretical study of ballooning modes and given the potential for such modes to adversely affect plasma performance, it is somewhat surprising that the experimental evidence for the existence of core localized high-n modes in tokamak plasmas is still very limited. Part of the experimental difficulty is that edge magnetic probes are expected to be rather insensitive to high-n core localized fluctuations. Consequently, edge magnetic diagnostics may not be as effective as density or temperature measurements in identifying weak high-n modes in the interior of large plasma devices such as the Toroidal Fusion Test Reactor (TFTR).

In this paper we present evidence for a ubiquitous band of high frequency modes in the core of neutral beam heated plasmas on TFTR. The evidence is mainly based on reflectometer and ECE measurements of density and temperature fluctuation, respectively. The main characteristic of the modes are that they propagate in the ion diamagnetic drift direction, appear as multiple peaks in the frequency spectrum within the range 50-150 kHz and have dominant toroidal mode numbers in the range $4<n<10$. The modes are highly localized (5-10 cm radial extent), and are usually observed near the $q=1$ radius with fluctuation levels $\tilde{n}/n,\ \tilde{T}_e/T_e<1\%$. Two distinct varieties are identified corresponding to a flute-like mode predominantly appearing around the $q=1$ radius and an outward ballooning mode appearing near the peak of the pressure gradient in the region $1<q<1.5$. The flute-like modes are predominantly observed in moderate performance supershots plasmas with $\tau_E<2\tau_L$, while the ballooning modes are mainly observed in higher performance discharges with $\tau_E>2\tau_L$. Although these two modes appear with similar frequencies and mode numbers, they are rarely observed in the same discharge. Unlike the

toroidally localized high-n ($10 < n < 15$) modes which are sometimes observed as a precursor to high-β disruptions and which are usually phase locked to an n=1 internal kink [1], these modes are more ubiquitous in typical supershot plasmas, have lower dominant n-numbers ($4 < n < 10$), shown no sign of toroidal localization or phase locking, and their onset does not appear to strongly limit plasma performance.

The paper is organized as follows. Section II discusses the flute like modes observed around $q \approx 1$ in moderate performance supershot plasma on TFTR. Section III discusses the more ballooning-like activity observed in higher confinement discharges in the region $q > 1$. A discussion of the results and comparison with high frequency modes observed on other machines such as PDX, DIII-D and PBX-M is presented in Sec. IV, followed by our conclusions in Sec. V.

II. Flute-like modes

Neutral beam heated discharges in the supershot regime on TFTR are characterized by highly peaked pressure profiles, sawtooth stable operation, high central ion temperatures ($T_i / T_e > 1$) and low edge recycling [13]. The evolution of the central plasma parameters and confinement time are shown in Fig. 1 for a supershot discharge with the following parameters: P_{NB}=15 MW, B_{TF}=4.5 T, R=252 cm, and I_P=1.6MA (shot #79099). The data indicates sawtooth free operation after 4.0 s. with $\tau_E \approx 2\tau_L$ and $T_i(0) \sim 3 \times T_e(0)$. Fig. 2 shows the amplitude spectrum of density, temperature and magnetic fluctuations taken over a 20 ms interval at 4.4 s into the discharge. The spectrum of density fluctuations in Fig. (2a) is obtained from an X-mode microwave reflectometer operating at 135 GHz with a plasma cutoff at $R \approx 290$ cm. The phase of the reflected wave is used to infer the density fluctuation level at the cutoff assuming the validity of 1-D geometric optics for long wavelength modes [14,15], and an rms density fluctuation level $\tilde{n} / n \sim 0.01$ is obtained over the range 50-150 kHz. This is comparable to the local temperature fluctuation level $\tilde{T}_e / T_e \sim 0.01$ estimated from the spectrum of Fig. (2b), taken using the multi-channel grating polychromator (GPC) diagnostic for second harmonic electron cyclotron emission from $R \approx 290$ cm [16]. These modes typically appear in equal frequency intervals with the dominant activity around 50-100 kHz and progressively weaker activity beyond 100 kHz. Lower frequency activity can also be observed at varying levels relative to the high frequency modes. Edge magnetic pickup coils normally observe only the lowest frequency components of the spectrum, corresponding to toroidal mode numbers n=1, 2 as shown in Fig. (2c). The radial displacement for the dominant mode in the spectrum at ~96 kHz is displayed in Fig. 3. The radial displacement ξ_r is obtained from GPC measurements on the high and low field side of the magnetic axis and is estimated using the relation $\xi_r \approx (\tilde{T}_e / T_e) L_T$, where L_T is the radial electron temperature scale length. Although the mode width is within the limit of the spatial resolution of the GPC diagnostic (~5 cm), the similar amplitudes on the low and high field side of the magnetic axis has been consistently observed on

TFTR. The radial displacement for the dominant modes in the spectrum rarely exceeds 0.1 cm. The *q*-profile in Fig. 3 is obtained from the TRANSP analysis assuming neoclassical resistivity [17]. The peak of the displacement appears to be localized near or slightly inside of the $q = 1$ surface, however the precision of the *q*-profile estimate from TRANSP is uncertain and cannot be relied upon for an accurate estimate of the mode rational surface.

A more effective method of identifying the mode rational surface is obtained from measurements of the toroidal and poloidal mode numbers of the fluctuations and from their spatial coincidence with other low frequency MHD activity. Although the high frequency modes are not observed on edge magnetic pickup coils, toroidal mode numbers may still be obtained from the cross correlation between toroidally displaced temperature and/or density measurements on the machine mid plane. Fig. 4 shows the relative phase versus frequency obtained from the cross spectrum between two GPC channels measuring the second harmonic cyclotron emission from the same radial location R~290 cm but displaced toroidally by $\Delta\phi = 124°$. Superimposed on the phase spectrum is the amplitude spectrum of the temperature fluctuations from one of the GPC channels which shows the location of the various spectral peaks. The data indicates that the relative phase between the two GPC channels increases linearly with frequency in increments of ~124°, which is consistent with toroidal mode numbers starting from n=1 at ~16 kHz and increasing in increments $\Delta n = 1$ up to n=10 or more. The dominant modes are at ~80 kHz and ~96 kHz correspond to toroidal mode numbers of n=5 and n=6 respectively. The analysis suggests that the toroidal mode numbers may extend up to $n = 20$ with frequencies above 200 kHz on some occasions, but at much reduced amplitudes relative to the dominant modes. Although the amplitude of the n=2, 3, 4 modes are quite low, the coherence is sufficiently high to give a reliable phase measurement. The relative phase between the two GPC channels at the same toroidal location but on the high and low field side of the magnetic axis (at R~255 cm and R~290 cm respectively) reveals ~0° and ~180° phase shifts for even and odd n-numbers, respectively. Although the poloidal mode number m can not be determined uniquely from midplane measurements alone, the parity of the mode (even or odd m) may be determined from the relative phase. The data appears consistent with m and n both even or both odd up to the highest observed mode frequencies, and the spatial coincidence of the all the modes strongly suggests that $m = n$ with the rational surface at $q = 1$. The lowest frequency modes observed on the magnetic pick up coils reveals $n = 1$ and $n = 2$, consistent with GPC estimates of the toroidal mode numbers. Note that the symmetry of the mode displacement on the high and low field side of the magnetic axis together with the narrow radial mode width ($\Delta r < 5$ cm) strongly suggests a flute-like mode with very long parallel wavelengths ($k_{\|} << 1/qR$).

From the estimate of the toroidal mode numbers, the real frequency of the modes in the plasma frame are found to closely correspond to half the local ion-diamagnetic frequency. The estimate of the mode frequency in the plasma frame depends on correctly subtracting the frequency shift induced by toroidal

plasma rotation. Both the toroidal velocity profile and the ion temperature profiles are measured using the CHERS diagnostic [18], and the ion diamagnetic frequency $\hat{\omega}_{*pi} = q\rho_i \upsilon_{ti}/rL_{pi}$ is evaluated using TRANSP run data, where $L_{pi}^{-1} = -d\ln p_i / dr$ is the ion pressure scale length, ρ_i and υ_{ti} are the ion larmor radius and ion thermal velocity, respectively. Here we have define $\hat{\omega}_{*pi}$ as the ion diamagnetic frequency corresponding to an *n*=1 mode at a minor radius r. The effective ion temperature for evaluating $\hat{\omega}_{*pi}$ is obtained from the *total* (beam+thermal) ion pressure divided by the total ion density. For modes propagating in the ion diamagnetic drift direction we expect the mode frequency to increase with co-plasma rotation where the co-direction refers to the direction of the plasma current. The frequency displacement between successive modes is plotted in Fig. 5 (solid circle) along with the plasma toroidal rotation frequency for an *n*=1 mode ($\hat{\omega}_\phi$), and the sum of the toroidal rotation and diamagnetic frequencies ($\hat{\omega}_\phi + \hat{\omega}_{*pi}/2$) for the same discharge. The minor radius of r/a~0.23 corresponds to the location of the observed high frequency modes and is taken from the equilibrium analysis of TRANSP. The sum of the two frequencies seems to fit the observed mode frequency, suggesting that the modes propagate close to $n\hat{\omega}_{*pi}/2$ in the plasma rest frame. This is at least consistent with the frequency expected for kinetic ballooning modes driven by the bulk ion pressure [8,9,12]. One important caveat is that the poloidal $E \times B$ flow has not been taken into account since it is not currently measured on TFTR. However, observations of similar mode activity for a large number of supershot plasmas has not revealed a significant discrepancy between the real mode frequency and the ion diamagnetic frequency after accounting for the toroidal rotation. This possibly indicates that $\upsilon_\theta << r\upsilon_\phi / R$ in the central region of supershot plasmas where υ_θ, υ_ϕ refer to poloidal and toroidal rotation velocities, respectively.

The high frequency flute like modes typically saturate at rather low levels $\tilde{n}/n < 0.01$ and tend to occur in discharges where there are no simultaneous large amplitude low-*n* MHD activity present. This is especially true for the *m*=1/*n*=1 fishbone mode. Fishbones on TFTR typically produce no more than 1-2 % drops in the neutron source strength with each burst, and are not as deleterious to the fast ion confinement as those observed with perpendicular beam injection in PDX [19]. The fishbone activity on TFTR strongly damps the flute-like high frequency activity. Fig. 6 shows reflectometer data taken in a discharge with similar plasma parameters but during fishbone activity. The discharge parameters for Fig. 6 are very similar to those of Fig. 1 and the reflectometer data is obtained from a 135GHz channel with a cutoff located at R~290 cm. It is evident that the high frequency activity in Fig. (6a) is strongly suppressed during the fishbone bursts shown in Fig. (6b), but recovers within ~1-2 ms after the fishbone burst. It is interesting to note that the high frequency activity exhibits rapid amplitude bursting between the fishbones with a characteristic frequency of ~5 kHz. The bandwidth of the bursting behavior corresponds to the line width of the individual modes in the frequency spectrum, and the spectral line widths are usually significantly broader than the width of low-*n* MHD activity observed on edge pickup coils.

The suppression of the flute-like modes during the fishbone bursts may be due to the local flattening of the hot particle distribution induced by the fishbone activity. Both the suppression of high frequency activity and the rapid amplitude modulation of the individual modes suggests a possible resonant interaction with some component of the beam ion distribution. Although the flute-like modes often occur in plasmas with no fishbone activity, in cases where they are observed in the same discharge the high frequency activity is consistently observed to precede the fishbones. In this sense the mode activity has the occasional appearance of a precursor to the fishbones. This is analogous to some of the characteristics of high frequency oscillations observed on PDX [20] which has been the subject of considerable discussion in the literature [21,11]. We will return to this discussion later.

Of crucial importance is whether these modes only appear as the central region of the plasma approaches the critical pressure gradient for ideal high-*n* ballooning modes. Fig. 7 shows a plot of the measured plasma pressure gradient and the estimated critical pressure gradient p'_{cr} corresponding to the ideal stability boundary for the discharge of Fig. 1 at t=4.4 s. The gray region indicates the location of the observed mode activity. The estimate of the critical pressure gradient in the core region of TFTR is highly sensitive to small variations in shear, and so cannot be treated quantitatively. Nonetheless, a characteristic feature of supershot plasmas is that the core is almost always calculated to be close to the first stability boundary. This characteristic results from the strong central peaking of the pressure profile in the region of low shear and large aspect ratio. For a time it was thought that a correlation could be established between the appearance of these flute-like modes and the proximity of the plasma core to the first stability boundary, however it was soon apparent that similar mode activity also existed in much lower performance discharges well within the first stable region. One such case is discussed below.

A high frequency band of flute-like modes are routinely observed in relatively low performance supershot plasmas on TFTR. These plasmas are in the transitional phase between the L-mode and the regular supershot and are typically characterized by energy confinement times $\tau_E \leq 1.5\tau_L$ and often (but not always) display one or more of the following characteristics; very long sawtooth periods (>250 ms), fishbone activity, and occasional core localized β-collapses. Such gross MHD activity limits the central plasma pressure and maintains overall broader pressure profiles and lower confinement times. Fig. 8 shows the evolution of central plasma parameters for one such discharge with P_B=12 MW, B_{TF}=4.5 T, R=260 cm, and I_P=1.8MA. Note that the central temperature and density collapse at t~3.42 sec. is not a typical sawtooth event but takes place over a much longer time scale. The β-collapse is associated with the slow growth of an *m*=1/*n*=1 mode and unlike a sawtooth event the central pressure profile is not flattened within the *q*=1 radius. The confinement time for this discharge is ~150 ms or about $1.5\times\tau_L$ both before and after the β-collapse, where τ_L is indicated by the dashed line in Fig. 8. The spectrum of temperature fluctuations at R~283 cm from the GPC is shown in Fig. 9 along with the spectrum of edge magnetic fluctuations taken at t~3.64 s. Note that no significant activity is observed

in the spectrum of the temperature fluctuations below 50 kHz, whereas no activity is observed on the magnetic spectrum apart from a weak broad peak around 200 kHz. This ~200 kHz mode has already been identified as an edge localized n=0 mode in the Alfven range of frequencies and is discussed elsewhere [22]. The local fluctuation level integrated over the 50-150 kHz band of core modes corresponds to $\tilde{T}_e / T_e \approx 0.005$. The radial displacement obtained from GPC measurements is shown in Fig. 10 for the dominant mode at ~83 kHz in Fig. 9 together with the q-profile measured using the MSE diagnostic [23, 24]. The displacement on the high and low field side of the magnetic axis appears to peak just inside of the $q = 1$ radius, however the difference is only 3-4 cm which is within both the spatial resolution of the GPC and also the experimental uncertainties in the q-profile measurement. Again the radial mode width has an upper bound set by the GPC resolution of ~5 cm at full width half maximum. Although the mode amplitude appears even a little stronger on the high field side, analysis of the displacement in a range of discharges shows no significant in/out asymmetry for these modes. The modes at all frequencies are again all spatially coincident and all show roughly equal amplitude on both sides of the magnetic axis. The proximity of the local pressure gradient to the critical pressure gradient corresponding to the first stability boundary is shown in Fig. 11 at t=3.3 s just prior to the β-collapse. Note that while p'_{cr} is comparable to that shown in Fig. 7, the pressure profiles is considerably broader resulting in a significantly lower central pressure gradient. Operationally these discharges are in the low β range of the supershot with $\beta_N < 1$ where $\beta_N = \beta / (I_P / aB)$.

Mode activity throughout most of the discharge is observed on the reflectometer diagnostic with a cutoff layer located at R~283 cm near the estimated location of the $q = 1$ radius. The spectral history of the high and low frequency modes are shown in Fig. 12 together with the evolution of the central electron temperature and the time behavior of the mode amplitude in a 30 ms interval following the β-collapse. Even through the β-collapse the cutoff layer is calculated to shift by no more than a 2-3 cm as the central density (and temperature) changes by no more than 10% (c.f. Fig. 8) and at low density the X-mode cutoff location is predominantly determined by the magnetic field strength. From Fig. (12b) it appears that the central collapse is associated with the slow growth of a low level $n = 1$ mode propagating originally in the ion diamagnetic drift direction. For the high frequency modes, assuming a mode width of ~5 cm, we estimate an integrated fluctuation level $\tilde{n} / n \sim 0.003$ over the bandwidth 50-100 kHz just prior to the β-collapse and $\tilde{n} / n \sim 0.01$ at the peak of the mode amplitude in the recovery phase after the collapse, as show in Fig. (12a).

The transient appearance of enhanced mode activity along with a down shift in the mode frequency is often observed after such a central β-collapse. The frequency variation of -20% takes place in a time interval in which the density is only changing by +5%, making it unlikely that the variation is due to a local change in the Alfven velocity. Also, CHERS measurements indicate a possible decrease in the central toroidal rotation velocity, although the level of variation is close to the limit of the diagnostic

resolution. Although toroidal mode numbers were not available from ECE measurements, we were still able to estimate the *n*-numbers from the rate of change of the mode frequencies after the β-collapse. Making use of the spatial coincidence of the modes and assuming they propagate with the same local phase velocity, we may use the relation

$$(n_0 + \Delta n)/n_0 = \left(\frac{\delta\omega}{\delta t}\right)_{n_0+\Delta n} \Big/ \left(\frac{\delta\omega}{\delta t}\right)_{n_0} \qquad ; \qquad \Delta n = 1,2,3...$$

to estimate the toroidal mode numbers. Here n_0 refers to the toroidal mode number of the lowest frequency mode in the spectrum at t=3.525 s and $(\delta\omega / \delta t)_n$ represents the rate of change of frequency for a given mode *n* at that time. Assuming the toroidal mode numbers increase in steps of $\Delta n = 1$ between successive peaks, the first four estimates of n_0 are shown in Table 1 and yield an average of $n_0 = 4 \pm 0.5$. The data is consistent with the toroidal spectrum *n*=4,5,6... as indicated by the dashed curves in Fig. 12. The spatial coincidence of all the modes down to the lowest mode numbers strongly suggests that the rational surface is at *q*=1. Note that the *m*=3/*n*=4 surface does not exist and the *m*=5/*n*=4 rational surface is significantly displaced from the point of observation according to the MSE measurement of the *q*-profile. Interestingly, $\hat{\omega}_{*pi}$ is observed to change very little through the discharge, and a comparison of the mode frequency (normalized to *n*=1) and the sum of plasma toroidal rotation and diamagnetic frequencies ($\hat{\omega}_\phi + \hat{\omega}_{*pi}$ / 2) is shown in Fig. 13. Again, good agreement between the observed mode frequency at R~280 cm and the sum $\hat{\omega}_\phi + \hat{\omega}_{*pi}$ / 2 is found. Note that the diamagnetic and rotation frequencies are plotted for times prior to the β-collapse and during the peak mode activity immediately after the central β-collapse, clearly indicating the weak effect of the collapse on the plasma toroidal rotation and ion diamagnetic frequency. It is of interest to note that ideal 2D-MHD calculations using the PEST II code [25] predicts unstable flute-like modes with 7<*n*<12 near q=0.9 just before the β-collapse. We will return later to a discussion of the PEST II analysis.

III. Ballooning-like modes

Given the appearance of high-*n* activity in low performance supershot plasmas it was not recognized for some time that high-*n* activity in high performance discharges could be qualitatively quite different. It now appears that two distinct kinds of mode activity are observed on TFTR, which we denote as flute-like and ballooning-like, which tend to occur in quite different parameter regimes. Fig. 14 shows the evolution of the central density $n_e(0)$ and density peakedness $n_e(0) / \langle n_e \rangle$, where $\langle n_e \rangle$ is the volume average density, for two discharges with identical machine parameters but with very different performance levels (central peaking and confinement times). The machine parameters are P_B=16 MW, B_{TF}=5.0 T, R=252 cm, and I_P=2.0 MA with $T_e \sim 10$ keV and $T_i \sim 30$ keV between 4.2 sec. and 4.6 sec. The main difference between the two discharges is the peaking of the central pressure between 4.2

and 4.6 sec. which comes mostly through the increase in the central density and density peaking as shown in Fig. 14. Note that the low performance discharge shows strong indications of a roll over in the evolution of the central density and temperature at t~4.2 s, while no roll over is observed in the high performance discharge. Fig. 15 displays the temperature and magnetic fluctuation spectra for the two discharges from GPC and edge magnetic measurements. The spectrum of Fig. (15a) is measured at R~280 cm in the degraded performance discharge with $\tau_E \sim 180$ ms, while Fig. (15b) corresponds to the spectrum of fluctuations measured at R~295 cm in the high performance discharge with $\tau_E \sim 230$ ms. The calculated *q*-profiles for the two plasmas are quite similar according the TRANSP analysis and the appearance of low-*n* MHD activity on the GPC in similar discharges indicates that R~280 cm is close to the $q = 1$ surface while R~295 cm is close to the $q = 4/3$ rational surface.

The spectral characteristics of fluctuations in Fig. (15a) are identical to the flute-like modes discussed in the previous examples with no observable magnetic fluctuations at high frequency and equal spacing between the spectral peaks. In contrast, the typical characteristics of the high frequency activity in high confinement discharges such as in Fig. (15b) are observable edge magnetic fluctuations, unequal frequency spacing between the spectral peaks and a significant enhancement of the mode amplitude on the low field side of the magnetic axis. Fig. 16 shows a comparison of the mode radial displacement from the GPC for the two cases, showing the larger radial location of the *n*=5 mode at ~96 kHz in Fig. (15b) relative to the more symmetric *n*=5 mode at ~94 kHz in Fig. (15a). From Fig. 16, the *n*=5 mode width in the high performance discharge is ~7-8 cm, while mode widths of up to 10 cm have been identified in other plasmas. The frequency difference between successive toroidal mode numbers are more irregular than for the modes nearer to $q = 1$ and closer examination reveals that their spatial localization are slightly different, with the higher toroidal mode numbers appearing at slightly smaller minor radius. This is consistent with $\omega_r \approx n(\hat{\omega}_\phi + \hat{\omega}_{*pi}/2)$ where $\hat{\omega}_\phi$ and $\hat{\omega}_{*pi}$ vary slightly depending on the precise mode location. Fig. 17 shows the experimentally measured average frequency per toroidal mode number (solid circle) plotted against the estimated toroidal rotation and ion diamagnetic frequency. Again, to within the precision of these measurements the agreement between the sum of the two frequencies and the observed mode frequency is extremely good. More importantly, the magnitude of the local toroidal rotation frequency is considerably lower than the diamagnetic frequency in this example, making it particularly clear that plasma rotation cannot account for the observed mode frequency. Fig. 18 shows the estimated plasma pressure gradient (solid line) compared with the calculated critical pressure gradient (dashed line) for ideal high-*n* ballooning modes. The figure indicates that the plasma core is close to the first stability boundary around the 5/4 and 4/3 mode rational surfaces near the observed mode location at r/a~0.3, whereas the lower performance plasmas tend to have profiles which are closest to the first stability boundary only within the *q*=1 radius (c.f. Fig. 7). Whether or not the plasma has locally crossed into the ideal unstable region is uncertain, given the sensitivity of the stability boundary to small variations in the local shear in the central region of the discharge. Nonethe-

less, plasmas which exhibit ballooning-like activity are systematically closer to the calculated first stability boundary in the region $1<q<3/2$ than lower performance discharges which only exhibit the flute-like activity around the q=1 radius. An important issue is what determines the dominant toroidal mode numbers observed in these plasmas. It is well know that mode numbers in the intermediate range $5<n<10$ should be even more stable than the high-n limit within ideal MHD [26], so why are not higher toroidal mode numbers observed? The influence of kinetic effects is a strong possibility such as FLR stabilization in very hot highly peaked plasmas, and energetic beam ion resonances during strong auxiliary heating. These effects will be discussed later. Finally, Fig. 19 displays the mode frequency in the plasma rest frame ($\hat{\omega}_r = \omega_r / n - \hat{\omega}_\phi$) against the local ion diamagnetic frequency for a range of high to moderate performance supershot plasmas covering the parameters in the present study with $B_T \sim 4.5 - 5.0$ T, $P_{NB} \sim 10 - 20$ MW, $R_0 \sim 252 - 260$ cm and $I_P \sim 1.6 - 2.0$ MA. To a good approximation both the q>1 ballooning-like modes in the high performance discharges (solid circles) and the q~1 flute-like modes in more moderate performance discharges (open circles) have a real frequency close to $\omega_r \approx \omega_{*pi} / 2$.

Occasionally the ballooning-like modes are observed prior to a minor or major disruption in high performance discharges on TFTR [1] and in many cases these modes appear to be phase locked to a large amplitude n=1 mode. A recent study of the disruption limit on TFTR showed that the maximum achievable β_N in a supershot is a strong function of the pressure peaking [27]. The product $\beta_N \cdot n_e(0) / \langle n_e \rangle$ is found to be a much better indicator of the beta limit on TFTR than β_N alone, so that paradoxically the highest confinement supershots which have the highest central density and pressure peaking also have some of the lowest β_N disruptions. An interesting issue which has still not been fully resolved is whether the rapidly growing high-n modes are indicative of the plasma locally crossing the ideal stability boundary, perhaps assisted by the non-axisymmetric perturbation produced by the strong n=1 instability. The fact that the β-limit on TFTR seems to depend on the central peaking is certainly suggestive of such a scenario. However, the rapid growth and large amplitude of these modes prior to disruptions on TFTR appears qualitatively different from the more ubiquitous low level activity discussed in this paper. The observation of ballooning like modes with $\omega_r \approx \omega_{*pi} / 2$ reported in this paper appears to be a rather benign indicator of enhanced plasma performance in the supershot regime. Possible exceptions to this are observations in several DT discharges of enhanced alpha losses correlated with ballooning-like activity [28] and very high-n ballooning-like modes ($13 < n < 60$) observed at the soft β-limit in high q_0 ($q_0 > 2$) high $\varepsilon\beta_\theta$ (≈ 0.7) plasmas on TFTR [29].

IV. Discussion

The flute-like and ballooning-like modes propagate in the ion diamagnetic drift direction with real frequencies $\omega_r \sim n\hat{\omega}_{*pi} / 2$, strongly suggesting that the main drive comes from the bulk ion pressure.

The flute-like activity occurs in sawtooth stable discharges with moderate levels of confinement ($\tau < 2\tau_L$) whereas the ballooning-like activity is more closely associated with high performance discharges ($\tau > 2\tau_L$) where the plasma is typically close to the ideal high-*n* stability boundary for *q*>1. The characteristics which distinguish the flute like modes are the equal amplitude on the high and low field side of the magnetic axis and the very narrow mode widths (<5 cm). These characteristics together with the appearance of mode activity in low to moderate performance supershots, are very similar to the characteristics expected for the Mercier modes with *q*<1. The only apparent requirement for the onset of mode activity is sawtooth stable operation and confinement times significantly above L-mode. A recent analysis of the equilibrium in Fig. 11 using the PEST II code suggests that the most unstable ideal flute-like (Mercier) modes have *n*=6,7 and appear just inside the *q*=1 surface with poloidal mode numbers *m*=5,6 respectively. Even though non-ideal effects are not included in the PEST analysis such as FLR stabilization [30,31], the correspondence of the calculated mode numbers with those observed in the experiment, the obvious lack of ballooning structure and the proximity of the modes to the *q*=1 surface are all rather encouraging agreements with the data. However there are several significant disagreements between the numerical analysis and the data. First, the modes on TFTR are clearly localized to $q = 1$ while the PEST II code predicts localization within the *q*=1 surface. Second, perhaps the most important discrepancy is that at large aspect ratio an increase in pressure should be destabilizing to the Mercier modes, whereas we clearly see no flute-like activity in the core of the most strongly peaked high confinement discharges on TFTR.

The similarity of some of the flute-like modes observed on TFTR to the fishbone precursor modes observed on PDX is very striking [20]. In most cases the high frequency activity on TFTR is observed to precede the onset of fishbone activity, or in the absence of fishbones to exist in plasmas that are free of sawteeth. Most often the onset of fishbone activity completely suppresses the high frequency modes. In such cases the high frequency activity appears as a precursor to the onset of fishbone activity. Occasionally the high frequency modes appear in between individual fishbone bursts as in Fig. 6 and in such cases the high frequency activity appears as a precursor to individual fishbone bursts. Some of the general features of the precursor modes on PDX are: (i) the mode activity occurs with 2<*n*<6 and real frequencies at multiples of the n=1 frequency; (ii) the activity is localized inside *r/a*=0.5, and most probably close to the *q*=1 surface; (iii) when the high-*n* activity occurs in discharges with fishbones, it generally appears as a precursor; (iv) when the activity occurs in the absence of fishbones it generally appears in sawtooth stable discharges; (v) the modes typically occur in 'high power' discharges with large $\varepsilon\beta_\theta$. Probably the equivalent of high power operation on PDX is any moderate supershot plasma on TFTR with suppressed sawteeth. It was pointed out by Weiland and Chen [21] that the high frequency activity on PDX could be possible evidence for KBMs driven by the precessional trapped beam ions. This would be consistent with the mode frequencies appearing at multiples of the *n*=1 frequency, assuming that the fishbones are also strongly driven by the precessional beam ions [32]. The only problem with this neat picture was the appearance of the modes as precursors to the fishbones in high

power discharges. A major concern with the KBM model was that the high-n kinetic ballooning modes should have a higher threshold for instability than the fishbone mode and so should not be observed as a precursor to the fishbones in high power discharges. The experimental data was reconciled with the theory by arguing that $q(0)$ is greater than one and dropping during the beam heating phase. The high-n kinetic ballooning modes are most likely localized outside the q=1 surface and the onset of fishbone activity would conveniently occur when $q(0)$ dropped below unity on axis. Of course, all this was pure conjecture as the q-profile, the location of the precursor and its detailed structure were unknown. The prevailing view at the time was that discharges free of sawteeth and fishbones must have $q(0)>1$. However, we know from MSE measurements on TFTR that the flute-like modes appear at the q=1 surface well before the onset of fishbones in sawtooth stable discharges. The similarities with the mode characteristics on TFTR may suggest that the PDX high frequency activity is more indicative of flute-like modes localized to the q=1 surface. The observations on TFTR are consistent with the high frequency activity having a lower threshold for instability than the fishbones, and then being rapidly suppressed by the onset of fishbone activity. The suppression of the flute-like modes probably occurs through the local flattening of the energetic particle distribution around the q=1 surface induced by the much larger amplitude fishbone bursts. Such a model is entirely consistent with the experimental observations on PDX during high power operation, and recent kinetic theory has also suggested alternative particle resonances which could significantly lower the critical beta for the onset of high-n instabilities [11].

A resemblance also exists between the spectrum of flute-like modes observed on TFTR and the pressure driven modes observed in non-axisymmetric equilibria on PBX-M [33]. A prominent feature of the PBX-M modes is that they appear in high β plasmas with very large amplitude m=1/n=1 modes which distort the axisymmetric equilibrium. In this new non-axisymmetric equilibrium, the low level high-n modes are all phase locked to the n=1 mode and show a strong ballooning feature on the low field side of the magnetic axis, similar to the mode activity observed prior to high β disruptions on TFTR [1]. The n=1 mode is thought to be stationary in the PBX-M plasma frame and is only Doppler shifted by toroidal plasma rotation. In contrast, the flute-like modes on TFTR seldom appear during strong core localized MHD activity and do not exhibit significant mode locking to other high frequency modes or to low-n MHD activity. When the n=1 mode is observed together with the high-n activity, typically at low amplitude, it too propagates with the ion diamagnetic frequency in the plasma rest frame. The lack of a strong ballooning feature to the $q = 1$ modes on TFTR adds a further discrepancy with the mode activity observed on PBX-M.

The ballooning-like modes for $q>1$ on TFTR are characterized by propagation in the ion diamagnetic drift direction, strong localization on the low field side of the magnetic axis and appear in high confinement discharges close to the first stability boundary for $1<q<1.5$. Most of the observations are close to the q=4/3 rational surface, which also corresponds near to the peak of the radial pressure gradient in

these discharges. Although the modes appear in highly peaked high confinement discharges, they do not necessarily appear in plasmas with high β_N. As pointed out earlier, the operational performance limits of TFTR supershot plasmas are better characterized by the parameter $\beta_N \cdot n_e(0) / \langle n_e \rangle$ than β_N alone [27], so that high confinement plasmas with strong central peaking tend to have a lower operational range of β_N. Although the mode observations are consistent with the picture of KBMs driven by the bulk ion pressure, some resemblance to the BAE modes observed on DIII-D may also be claimed [34]. The characteristics of the BAE modes are: (i) The mode frequency scales with the Alfven speed, (ii) The mode is only observed at high values of β_N, (iii) The mode frequency is typically 1/2 to 1/3 the TAE mode frequency. A major difference with BAE mode characteristics is that on TFTR there are a number of dominant modes with frequencies which scale proportionately with the toroidal mode number in the plasma rest frame. The mode frequencies can range from well below the TAE frequency up to values comparable to the TAE frequency ($\omega_{TAE} \sim 180 - 220$ kHz) [35], whereas the BAE gap modes have frequencies which are not expected to scale in proportion to the toroidal mode number.

A critical issue for the ballooning-like modes is their influence on plasma performance in TFTR. If the modes are driven by the local pressure gradient with real frequency $\omega_r \approx \omega_{*pi} / 2$, then they should have some effect on local thermal transport and on the transport of energetic particles which resonate with the mode. From Fig. 14 it is apparent that the central density and profile peaking continue to increase even after the onset of ballooning activity after 4.2 s in the high performance discharge, so it is apparent that the modes do not have the same catastrophic effect on the plasma performance as the ballooning activity observed prior to high-β disruptions [1]. Nonetheless, it is quite possible that as the central plasma pressure is increased or as the plasma is driven closer to the first stability boundary, that their effect on energetic particle transport and confinement may become more apparent. There is evidence for both enhanced local transport at the soft beta limit in TFTR induced by ballooning-like activity [29] and for enhanced losses of alpha particles in DT plasmas [28].

The remainder of the discussion will focus on possible non-ideal effects which may influence the mode characteristics observed on TFTR. An important issue is whether non-ideal effects, such as particle resonances or FLR stabilization, are influencing the range of dominant toroidal mode numbers of flute-like or ballooning-like activity observed on TFTR. We first consider the possible importance of FLR stabilization. Evaluating the gyroradius parameter $\Lambda = b / \varepsilon_p$ [30] for the discharges considered in this paper, where $b = k_\perp^2 \rho_i^2 / 2$, $k_\perp = nq / r$, and $1 / \varepsilon_p = R / L_{pi}$, gives values in the range $0.01 < \Lambda / n^2 < 0.05$. The lower and upper bounds are mostly determined from the local ion pressure scale length which can be as short as 15 cm in the core of high performance discharges on TFTR. In regions of low shear in the plasma core FLR stabilization can be important even for moderate values of Λ, ($\Lambda > 1$). Surprisingly, this would suggest significant FLR stabilization for n>10 in the core region of supershot plasmas on TFTR which is consistent with the range of observed dominant mode num-

bers. Further evidence which may support this possibility is the increased range of mode numbers and enhanced fluctuation levels observed in the flute like activity after a core β-collapse, as shown in Fig. 12. FLR stabilization may also provides a possible explanation for why the flute-like modes are not observed in the core of very high confinement discharges on TFTR. It should be noted that the influence of FLR effects on the stability of the intermediate range of mode numbers should properly be evaluated using realistic kinetic toroidal eigenmode calculations [36].

A further issue is whether resonant effects between beam ions and the high frequency activity may account for the range of dominant mode numbers observed on TFTR. Theory suggests that the KBMs could be destabilized by energetic particles provided the mode frequency matches either particle precessional frequency or the ion transit frequency and recent analysis has extended this picture to include both the ion bounce and precessional drift-bounce resonances [11]. Earlier results have even shown that the precessional drift resonance of thermal ions is sufficient to lower the threshold for instability provided $\overline{\omega}_d \sim \omega_{*pi}$ [9,37]. More recently, 1D-kinetic codes [38] have been extended to fully toroidal 2D geometries which will hopefully address the intermediate range of mode numbers observed on TFTR [36]. A common theme in all this work is that the kinetically driven ballooning modes can appear below the ideal MHD threshold but with much reduced growth rates (and hence lower saturated amplitudes) than the ideal unstable modes. Although it is difficult to determine with any precision the location of first stability boundary, the experimental observation of low level ballooning-like activity in high confinement discharges without severe effect on plasma performance is suggestive of possible KBM activity.

For the data obtained on TFTR, given that $\omega_r \sim n\hat{\omega}_{*pi}/2$, the real mode frequency is most likely not determined by the energetic beam ions. This rules out the class of 'beam' modes as a possibility [39]. The general expression for satisfying the wave transit resonance for a single *m* and *n* component of a particular mode is given by

$$\omega_r - \overline{\omega}_d \pm (m - nq)\omega_t = 0 \qquad (1)$$

where $\omega_r \approx \omega_{*pi}/2$ is the mode frequency, $\overline{\omega}_d$ is the transit averaged magnetic drift frequency, and ω_t is the ion transit frequency [12]. Here we assume that *m* and *n* represent the dominant Fourier components of the mode. Typically, $\overline{\omega}_d$ is negligible for passing particles on TFTR. For trapped particle resonances the condition is given by

$$\omega_r - \overline{\omega}_d + p\omega_b = 0 \qquad (2)$$

where

$$\overline{\omega}_d = \frac{nq}{r}\frac{cT_i}{eB_0}\frac{1}{R}$$

is the average precessional frequency, ω_b is the bounce frequency and typically $p = 0, \pm 1$ [12]. The tangentially oriented neutral beams on TFTR operate near $E \sim 105$ keV in both deuterium (D) and tritium (T). No significant difference in the mode frequencies or mode amplitudes have been observed in comparable DD, DT or TT plasmas where DD refers to all deuterium beam injection and DT refers to mixed D and T beams. From the TRANSP analysis of one of the high performance discharges considered in this paper (#77309) the average energy of a slowing down distribution of either D or T beam ions is 60 keV at the mode location r/a~0.34. This gives a beam ion transit frequency $\omega_t \approx \upsilon_{ti}/qR$ of ~110 kHz and ~90 kHz for the D and T beams, respectively. The 1/2 and 1/3 energy components of the neutral beam ions may be ignored as they do not penetrate into the central region of the discharge. The transit frequency of a full energy beam ion at 100 keV is also close to 100 kHz given that there is a relative angle of $\sim \pi / 4$ between the beams and magnetic field lines at the mode rational surface. In comparison, the bounce frequency of a beam ion $\omega_b \approx \sqrt{\varepsilon}\omega_t$ with $\varepsilon = r / R \approx 0.1$ is ~35 kHz for both D and T, while the precessional frequency for trapped beam ions at *r/a*~0.34 is around 3 kHz for *n*=1, again for both species. These figures are not expected to vary significantly for the plasmas parameters considered in this paper. Given that $\overline{\omega}_d << \omega_{*pi}$, the precessional beam ions are not likely to drive these modes. For flute-like modes with a single poloidal/toroidal mode number, from Eq. 1 the resonant condition can be satisfied for

$$w > \frac{1}{q'}\frac{\hat{\omega}_{*pi}}{\omega_t}$$

where w is the mode width and $q' = |dq/dr|$. For the flute-like modes in the low performance discharge of Fig. 8, taking $q' \approx 0.02$ / cm from MSE measurements, we obtain the resonant condition $w > 7.5$ cm while from Fig. 10 we obtain a crude estimate of the mode width of at ~ 5 cm. Thus, without a more sophisticated calculation, we can only conclude that the estimated mode width is of the order of the width required for the transit resonance to be possible. However, detailed numerical calculations using a slowing down distribution of beam ions are required in order to determine if such a resonance is likely for the flute modes. The bounce resonance has much greater difficulty fitting the experimental data, particularly given the number of modes and their range of frequencies. Note that for the flute modes, the transit resonance condition is essentially independent of the toroidal mode number and so does not account for the dominant range of mode numbers observed on TFTR. Nonetheless, the interaction of the fishbones with the high frequency activity and the irregularity of the mode amplitude variations shown in Fig. 6 are possible evidence for weak interaction with some component of the

circulating beam ions.

The situation is considerably different for the ballooning-like modes because of the strong coupling between different poloidal mode numbers which accounts for the observed outward ballooning feature. For such modes, taking $k_{\|} \sim 1/qR$ leads to the approximate transit resonant condition $\omega_r \approx \omega_t$ [10]. Such a resonance is now sensitive to the toroidal mode number and leads to a dominant mode number $n \sim 2\omega_{tr} / \hat{\omega}_{*pi}$. In most cases this corresponds to $n \approx 6$ which is consistent with the range of dominant mode numbers observed on TFTR. For example, the dominant *n*=6 mode in shot# 77309 has a real frequency in the plasma frame $\omega_r \approx 85$ kHz, which compares very well with the transit frequency of D or T beam ions. Thus, for the ballooning-like activity, it is plausible that the transit resonance play a significant role in determining the dominant toroidal mode numbers, while the trapped beam ions again appear much less likely to resonate with the modes. Further studies should focus on the possibility of modifying the transit frequency of the beam ions so as to more directly determine its influence on the spectrum of unstable modes, although it is operationally difficult to make significant changes to the neutral beam voltage.

V. Conclusions

Two distinct varieties of spatially localized modes in the range of intermediate toroidal mode numbers 4<n<10 are observed in supershot plasmas on TFTR. The first class of modes appears flute-like in character, with very narrow mode widths ($\Delta r < 5$ cm), rational surface close to *q*=1 and highly symmetric mode amplitude envelope on the low and high field side of the magnetic axis. The flute-like modes predominantly appear in lower performance supershot plasmas with $\tau_E < 2\tau_L$ and are readily stabilized by m=1/n=1 fishbones. The second class of modes mostly appear in high confinement plasmas with $\tau_E > 2\tau_L$, have mode widths ranging from ~5-10 cm, show enhanced amplitude on the low field side of the magnetic axis, and can sometimes be observed on edge magnetic pickup coils. Both sets of modes are found to propagate close to half the local ion diamagnetic frequency ($\omega_r \approx \omega_{*pi}/2$). The data indicates that FLR effects together with resonant circulating D or T beam ions may play a role in determining the spectrum of modes observed on TFTR. Much work still needs to be done in determining the nature and origin of these modes and their influence on core confinement, particularly at high beta. Further investigation should focus on the instability mechanism, and specifically if energetic beam ions are playing a significant role in determining the dominant mode numbers.

Acknowledgments

This work was supported by DOE contract # DE-AC02-76-CHO3073. One of the authors (R.N.) would like to thank Mike McCarthy for the continued reliability of the microwave reflectometer and to R.J.

Hastie for valuable discussions. The authors would like to thank the entire TFTR team for the successful operation of the machine.

References

[1] E.D. Fredrickson, *et al., Proceedings of the 15th IAEA conference on Plasma Physics and Controlled Fusion Research*, Seville, Spain, 26th Sept.-1st Oct. 1994; E.D. Fredrickson, K. McGuire, et al., Prin. Lab. Rep. PPPL-3023, Sept. 1994. (also submitted to Phys. of Plasmas, 1994; Y. Nagayama *et al*., Phys. Rev. Lett., **69**, 2376 (1992); Y. Nagayama *et al*., Phys. Fluids B, **5**, 2571 (1993)
[2] J.W. Conner, J.B. Taylor and M.F. Turner, Nuclear Fusion, **24**, 642 (1984)
[3] A. Sykes *et al*., in *Plasma Physics and Controlled Nuclear Fusion Research* (Proc. 7th International Conference 1978), Vol. 1 IAEA, Vienna (1979) p. 625
[4] H. Furth, J. Killeen, M. Rosenbluth and B. Coppi, *Plasma Physics and Controlled Nuclear Fusion Research,* (Proc. 2nd International Conference 1965), Vol. 1 IAEA, Vienna (1966) p. 103
[5] R.M. Kulsrud, *Plasma Physics and Controlled Nuclear Fusion Research,* (Proc. 2nd International Conference 1965), Vol. 1 IAEA, Vienna (1966) p. 127
[6] B. Coppi, Phys. Rev. Lett. **39**, 939 (1977)
[7] J.W. Conner, R.J. Hastie, and J.B. Taylor, Phys. Rev. Lett. **40**, 396 (1978)
[8] W.M. Tang, J.W. Connor and R.J. Hastie, Nuclear Fusion, **20**, 1439 (1980)
[9] C.Z. Cheng, Phys. Fluids, **25**, 1020 (1982)
[10] L. Chen, in *Theory of Fusion Plasmas,* edited by J. Vaclavik, F. Troyon, and E. Sindoni (Association EURATOM, Bologna, 1988), p. 327
[11] H. Biglari and L. Chen, Phys. Rev. Lett. **67**, 3681 (1991)
[12] S. Tsai and L. Chen, Phys. Fluids B Plasma Physics, **5**, 3284 (1993)
[13] J. Strachan *et al.*, Phys. Rev. Lett. **58**, 1004 (1987)
[14] R. Nazikian and E. Mazzucato, Rev. Sci. Instrum. **66**, 392 (1995)
[15] E. Mazzucato and R. Nazikian, Phys. Rev. Lett. **71**, 1840 (1993)
[16] A. Cavallo *et al*., Rev. Sci. Instrum. **59**, 889 (1988)
[17] R. V. Budny *et al*., Nuclear Fusion, **32**, 429 (1992)
[18] B.C. Stratton, R.J. Fonck, K.P. Jaehnig, N. Schechtman, E.J. Synakowski, *Proceedings of the IAEA Technical Committee Meeting on Time Resolved Two- and Three-Dimensional Plasma Diagnostics*, 78 (1991)
[19] K. McGuire *et al*., Phys. Rev. Lett. **50**, 891 (1983)
[20] K. McGuire *et al.*, Bull. Am. Phys. Soc. **28**, 1173 (1983)
[21] J. Weiland and L. Chen, Phys. Fluids **28**, 1359 (1985)
[22] Z. Chang, *et al*., Prin. Lab. Rep. PPPL-3115, July 1995 (also submitted to Nuc. Fusion, 1995)
[23] F.M. Levinton, et al., Rev. Sci. Instrum. **61**, 2914 (1990).

[24] F.M. Levinton, *et al.*, Phys. Fluids B, **5**, 2554 (1993)
[25] R.C. Grimm, R.L. Dewar, J. Manickam, J. Comp. Physics, **49**, 94 (1983)
[26] R.L. Dewar *et al.*, Nuclear Fusion, **21**, 493 (1981)
[27] D. Mueller, *et al.*, submitted to Fusion Technology, May 1995
[28] Z. Chang, *et al.*, submitted to Phys. Rev. Lett. (1995)
[29] S.A. Sabbagh *et al.*, Bull. Am. Phys. Soc. **38**, 1984 (1993)
[30] W.M. Tang, J.W. Connor, R.B. White, Nuclear Fusion, **21**, 891 (1981)
[31] W.M. Tang, R.L. Dewar, J. Manickam, Nuclear Fusion, **22**, 1079 (1982)
[32] L. Chen, R.B. White, and M.N. Rosenbluth, Phys. Rev. Lett. **52**, 1122 (1984)
[33] S. Sesnic, *et al.*, Nuclear Fusion, **33**, 1877 (1993)
[34] W.W. Heidbrink, *et al.*, Phys. Rev. Lett. **71**, 855 (1993)
[35] K.L. Wong *et al.*, submitted to Phys. Rev. Lett, 1995
[36] W.M. Tang and G. Rewoldt, Phys. Fluids B **5**, 2451 (1993)
[37] C.Z. Cheng, Nuclear Fusion, **22**, 773 (1982)
[38] G. Rewoldt, Nucl. Fusion, **31**, (1991).
[39] L. Chen, Phys. Plasmas **1**, 1519 (1994)

Figure Captions

Fig. 1. Time variation of plasma parameters: (a) neutral beam power, (b) energy confinement time, (c) central electron density, (d) central electron temperature and (e) central ion temperature obtained from CHERS.

Fig. 2. Spectrum of fluctuations taken at t=4.4 sec. and R=290 cm: (a) density fluctuation spectrum from the reflectometer, (b) electron temperature fluctuations from the GPC and (c) the magnetic fluctuation spectrum on edge pickup coils.

Fig. 3. Calculated *q*-profile from TRANSP and the radial displacement ξ_r inferred from GPC measurements of the dominant 96 kHz mode in Fig. 1. Very weak or no asymmetry is observed in the mode amplitude on the high and low field side of the magnetic axis.

Fig. 4. Relative phase between two toroidally displaced temperature fluctuation measurements (solid circles) plotted versus frequency and inferred toroidal mode number *n*. The two GPC diagnostics are separated toroidally by 124° and the increasing phase as a function of frequency indicates propagation

in the direction parallel to the plasma current (co-direction). Overlaid on the cross phase is the amplitude spectrum from one of the GPC channels (dashed curve) showing the location of the spectral peaks.

Fig. 5. Plot of toroidal rotation frequency ω_ϕ, and the sum of toroidal rotation and one half the ion diamagnetic frequency $\omega_\phi + \omega_{*pi}/2$ obtained from CHERS measurements, compared with the observed mode frequency per toroidal mode number $\hat{\omega} = \omega / n$ (solid circle). The rotation and diamagnetic frequencies are plotted between 4.2 -4.4 sec. in intervals of 0.1 sec.

Fig. 6. Reflectometer data taken of density fluctuations near q~1 shows evolution of high frequency modes $50-150$ kHz (a) during fishbone bursts $5-15$ kHz (b).

Fig. 7. Measured pressure gradient (solid line) and calculated stability boundary for ideal high-n ballooning modes (dashed line) at 4.4 sec into the discharge. The gray region corresponds to the mode location.

Fig. 8. Evolution of plasma parameters for a low performance supershot discharge with a central beta collapse: (a) beam power, (b) energy confinement time (dashed curve is the equivalent L-mode confinement time), (c) central electron density, (d) central electron temperature and (e) central ion temperature.

Fig. 9. Spectrum of (a) temperature fluctuations at R=283 cm from the GPC and (b) edge magnetic fluctuations approximately 150 msec. after the beta collapse.

Fig. 10. Measured q-profile from MSE (solid line) and inferred radial displacement for the dominant 83 kHz mode from the GPC (dashed curve) evaluated at t=3.65 sec. The mode displacement shows little difference between the high and low field side of the magnetic axis. The upper bound on the mode width is ~5 cm and is of the order of the separation between GPC channels.

Fig. 11. Measured pressure gradient (solid line) and calculated critical pressure gradient for ideal high-n ballooning modes (dashed line) at t=3.3 sec. just before the beta collapse. The data indicates that the plasmas is far from the first stability boundary.

Fig. 12. Contours of amplitude versus frequency and time for the spectrum of density fluctuations observed using the X-mode reflectometer @ 135 GHz with a cutoff located at $R \approx 283$ cm. The evolution of the high frequency modes (a); the evolution of the n=1 mode (b); and the central electron temperature (c); are shown through the central beta collapse. Mode numbers estimated from the time rate of change of frequencies after the collapse are shown in (a) and range from n=4 to n=10. A bursting behavior of the mode amplitude after the beta collapse is clearly indicated in (d).

Fig. 13. The frequency separation between successive toroidal mode number in Fig. 12 observed at $r/a = 0.22$ (solid circle) compared with the toroidal rotation frequency ω_ϕ and $\omega_\phi + \omega_{*pi}/2$ for four time slices; t=3.32, 3.42, 3.52, 3.62 sec.

Fig. 14. Beam power (a), evolution of central density (b) and density peaking $n_e(0)/\langle n_e \rangle$ (c) for two plasmas with identical machine parameters, P_B=16 MW, B_{TF}=5.0 T, R=252 cm, I_P=2.0 MA, $T_i \sim 30$ keV, $T_e \sim 10$ keV but with very different central density and profile peaking.

Fig. 15. Spectrum of electron temperature and magnetic fluctuations for the two discharges in Fig. 16 indicating flute like modes in (a) and ballooning like modes in (b) for the low and high performance plasmas respectively. The high-n ballooning like modes are readily observed on the edge magnetic coils and indicate toroidal mode numbers n=4,5.

Fig. 16. Estimated radial displacement of the dominant 95 kHz n=5 modes in the low performance plasma in Fig. 17 (a) (dashed line) and displacement for the dominant 96 kHz n=5 mode in the high performance plasma of Fig. 17 (b) (solid line). Observation of low order m=1/n=1 and m=4/n=3 mode activity on the GPC indicates that the flute like modes are localized to the $q=1$ region whereas the outward ballooning modes are localized near $q = 4/3$.

Fig. 17. Plot of toroidal rotation frequency ω_ϕ, and the sum of toroidal rotation and ion diamagnetic frequency $\omega_\phi + \omega_{*pi}/2$ for an n=1 mode, compared with the frequency separation between successive mode numbers (solid circle) for the spectrum in Fig. 17 (b). The rotation and diamagnetic frequencies are plotted between 4.2 -4.4 sec. in increments of 0.1 sec.

Fig. 18. Plasma pressure gradient (solid line) and calculated critical pressure gradient for ideal high-n ballooning modes (dashed line) at 4.45 sec in the enhanced performance discharge of Fig. 16. The central region of the plasma is close to the calculated ballooning boundary out to r/a~0.3 where the modes are located. The gray region indicates the mode location.

Fig. 19. Plot of the mode frequency in the plasma frame $\hat{\omega}_r$ against the inferred ion diamagnetic frequency $\hat{\omega}_{*pi}$ for flute like modes (open circles) and ballooning-like modes (closed circles). The frequencies are normalized to n=1. The region within the dashed lines corresponds to $\omega_{*pi}/2 < \omega_r < \omega_{*pi}$. The data indicates that both the flute-like and ballooning-like modes propagate near to $\omega_r \approx \omega_{*pi}/2$ in the plasma frame.

Table Captions

Table 1

Tabulation of mode number estimates based on the rate of change of frequency at t=3.525 sec. in Fig. 12. The first column represents the toroidal mode number n ranging from the lowest frequency mode n_0 to $n_0 + 4$; the second is the frequency variation ω'_n in kHz per 20 ms.; the third is the ratio of the frequency variations; and the fourth is the corresponding estimate of the toroidal mode number n_0. The data indicates $n = 4 \pm 0.5$.

n	ω'_n	ω'_n/ω'_{n0}	n_0
n_0	4.57	1.00	-
n_0+1	5.71	1.25	4.00
n_0+2	6.90	1.51	3.92
n_0+3	8.70	1.90	3.33
n_0+4	8.33	1.82	4.87

Table 1

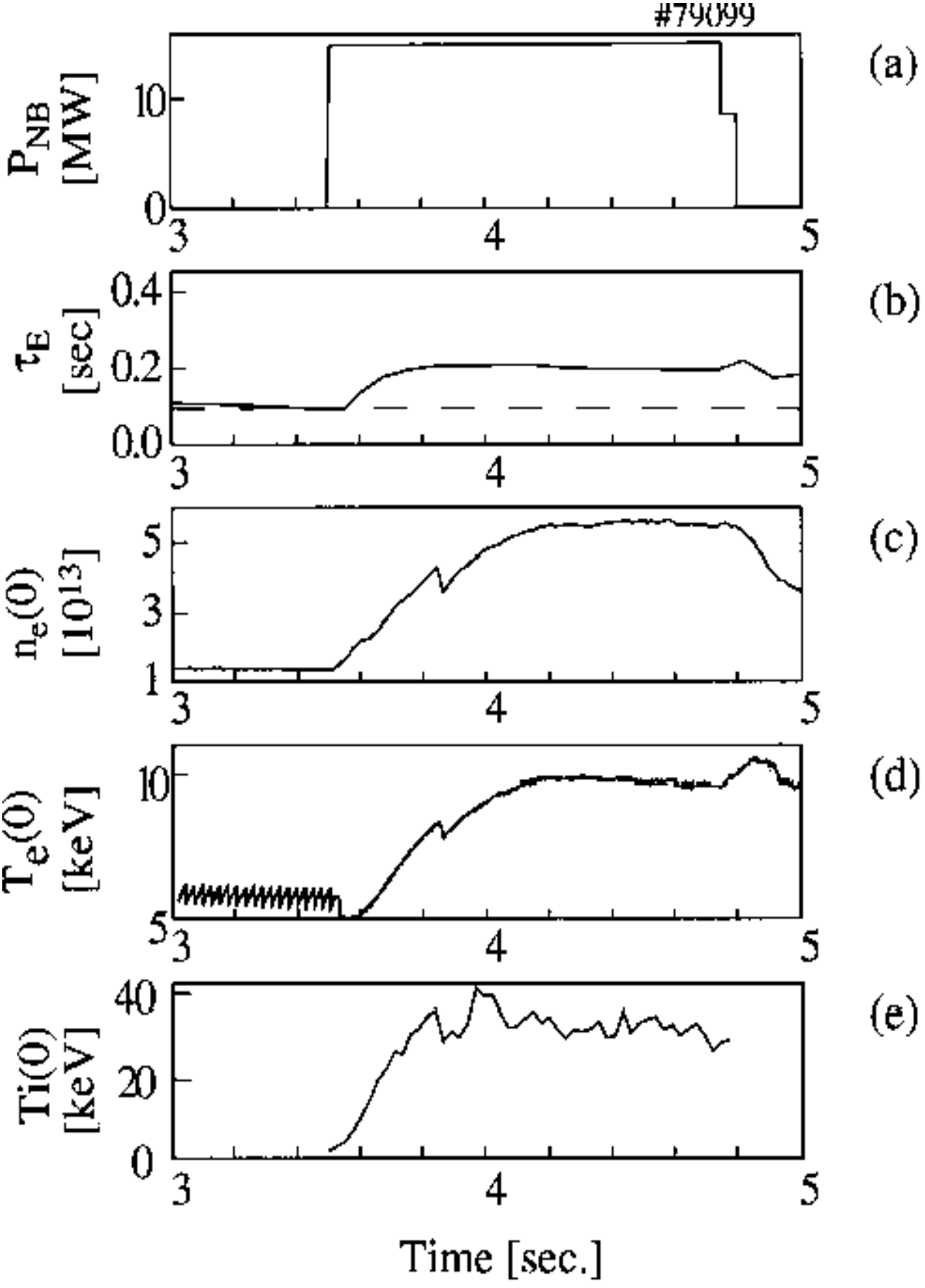
#79099
P_{NB} [MW]
10
0
3
4
5
(a)
τ_E [sec]
0.4
0.2
0.0
(b)
$n_e(0)$ [10^{13}]
5
3
1
(c)
$T_e(0)$ [keV]
10
5
(d)
Ti(0) [keV]
40
20
0
(e)
Time [sec.]

Fig. 1

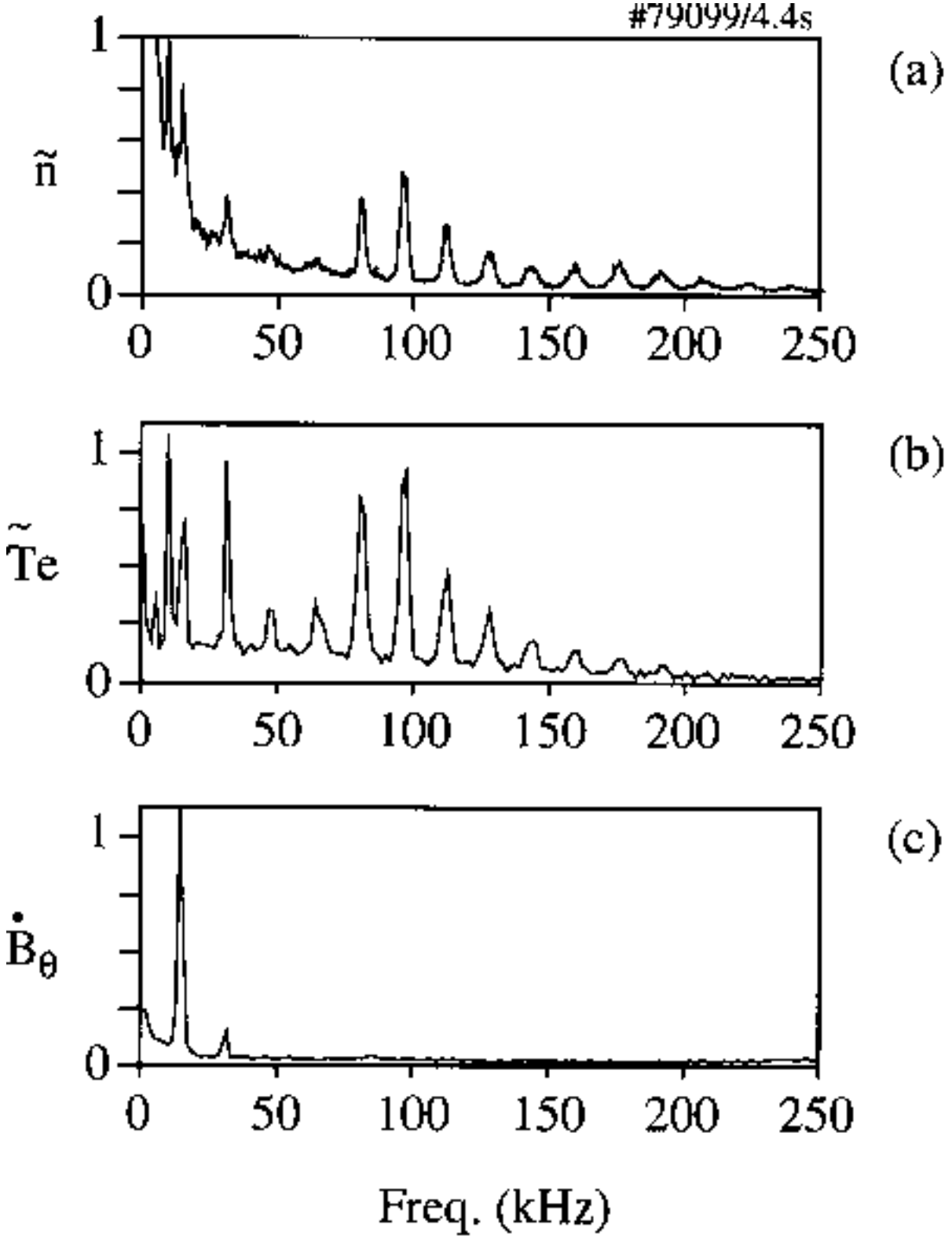
#79099/4.4s
(a)
$\tilde{n}$
1
0
0
50
100
150
200
250
(b)
$\tilde{T}e$
1
0
0
50
100
150
200
250
(c)
$\dot{B}_\theta$
1
0
0
50
100
150
200
250
Freq. (kHz)

Fig. 2

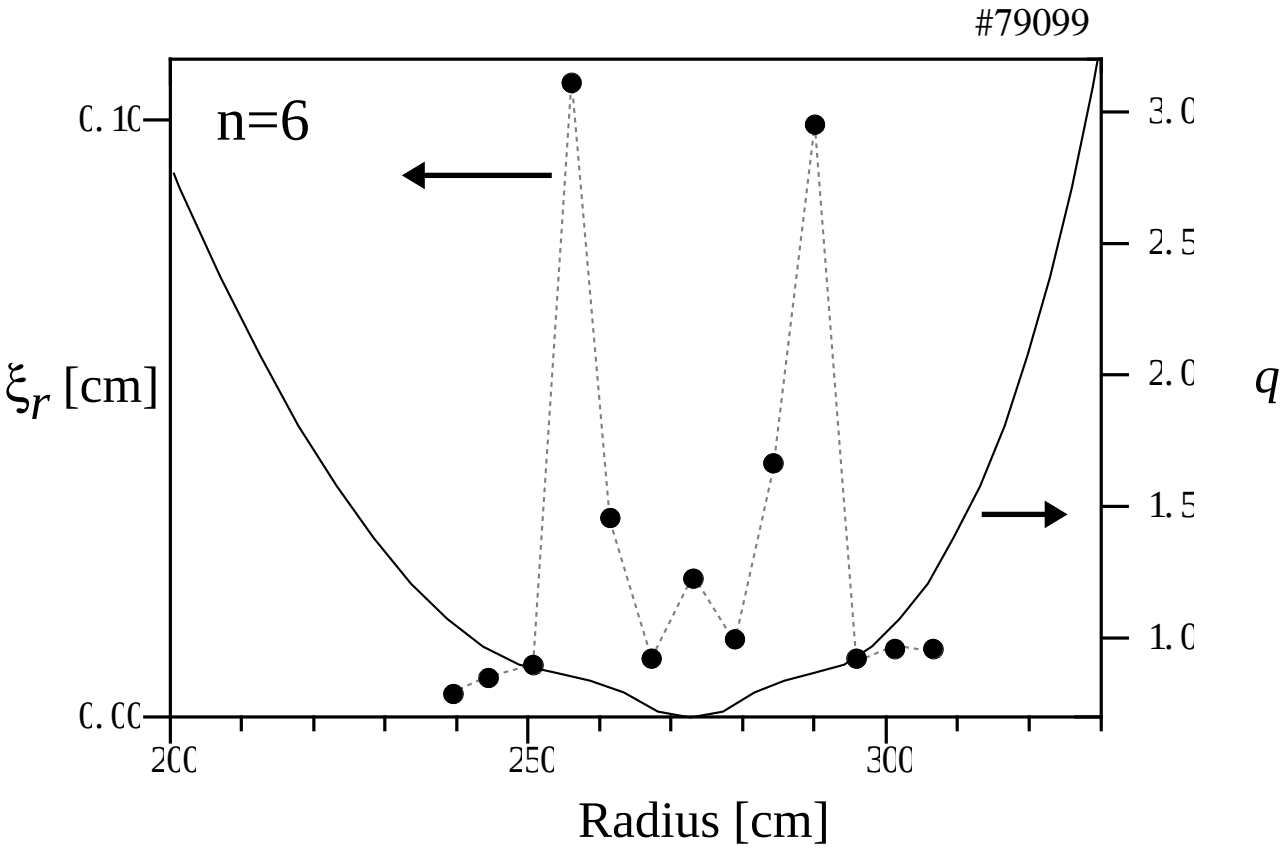

Fig. 3

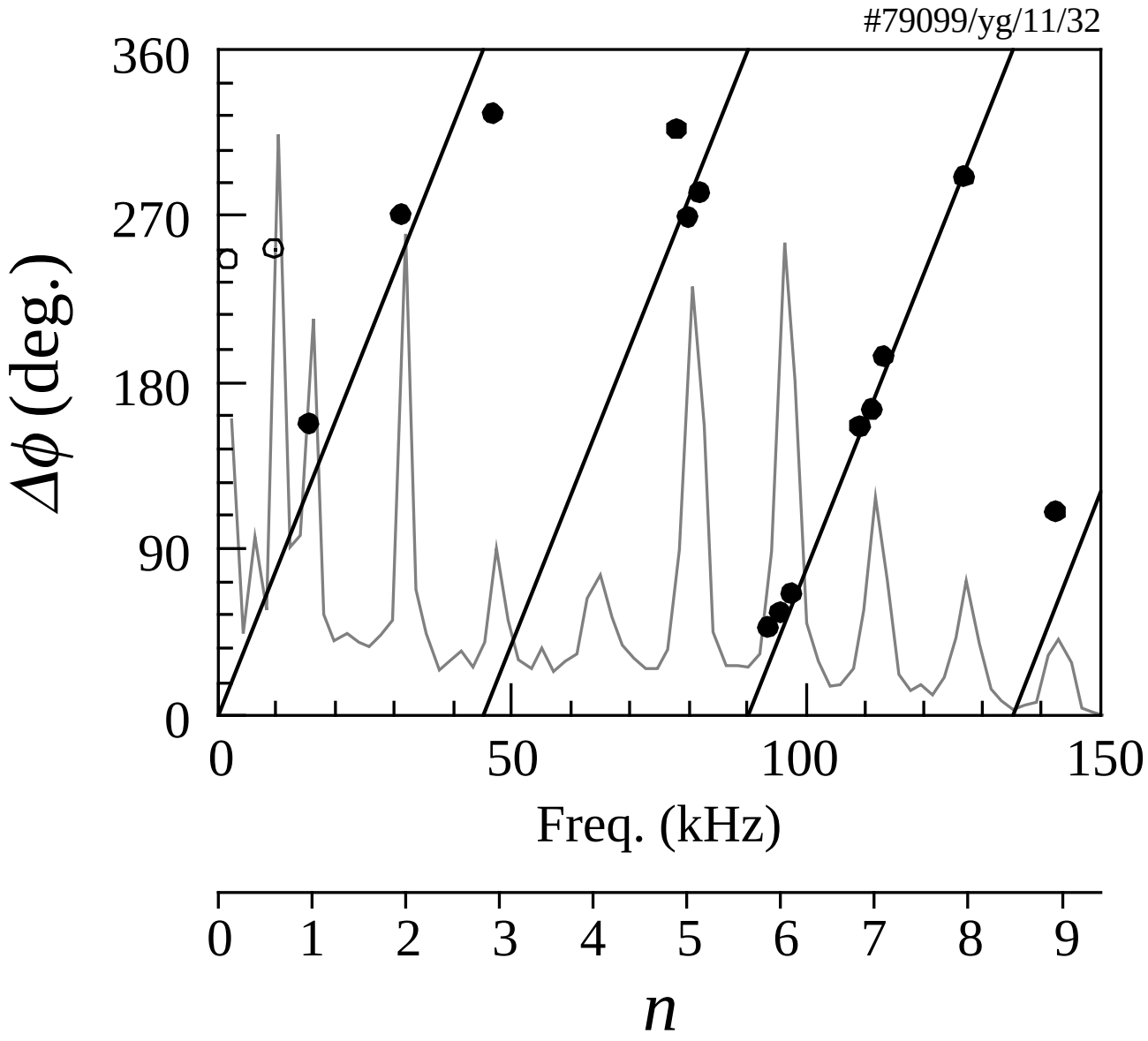
#79099/yg/11/32
360
270
180
90
0
Δφ (deg.)
0
50
100
150
Freq. (kHz)
0
1
2
3
4
5
6
7
8
9
n

Fig. 4

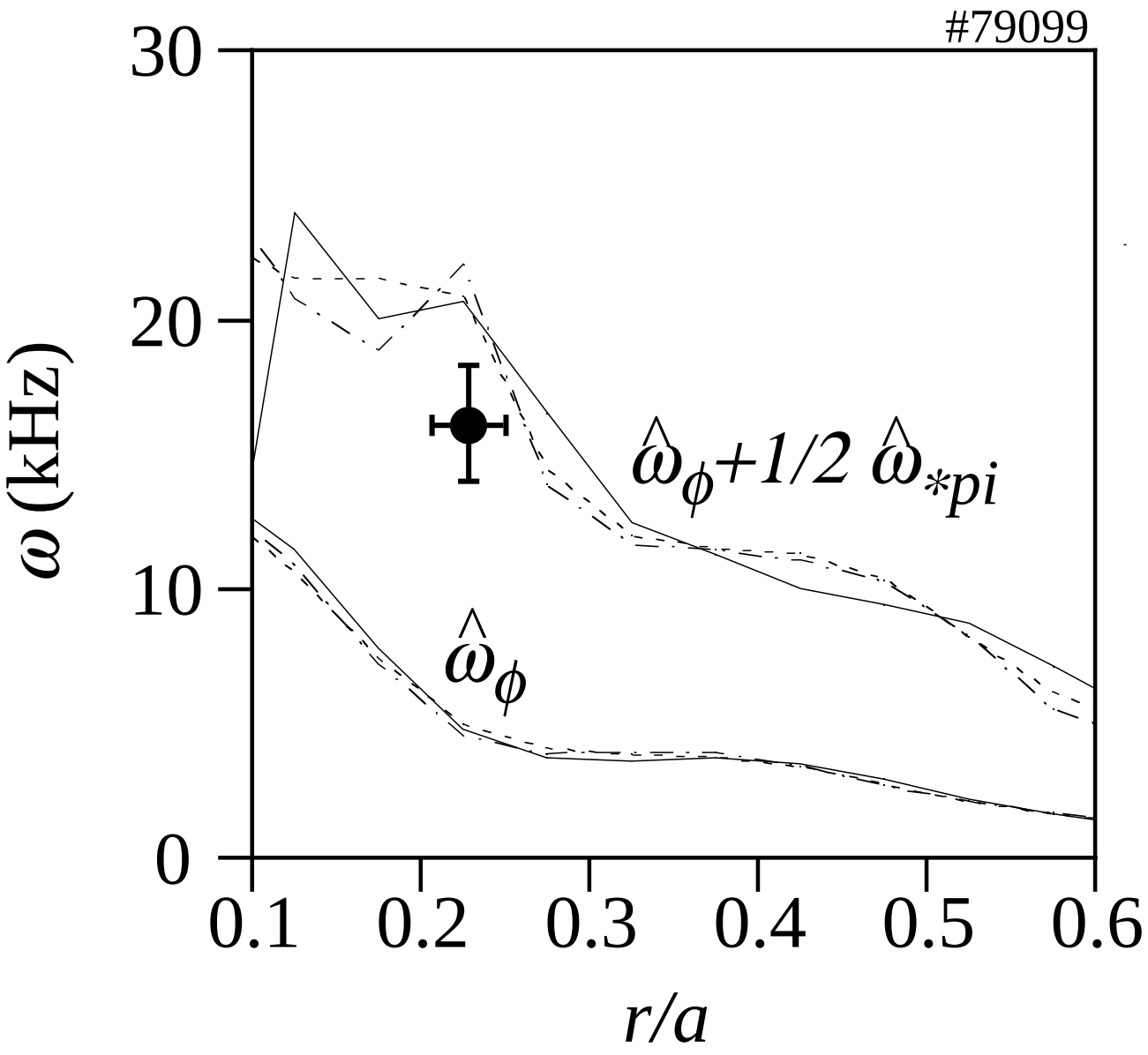
#79099
30
20
10
0
ω (kHz)
0.1
0.2
0.3
0.4
0.5
0.6
r/a
$\hat{\omega}_\phi$+1/2 $\hat{\omega}_{*pi}$
$\hat{\omega}_\phi$

Fig. 5

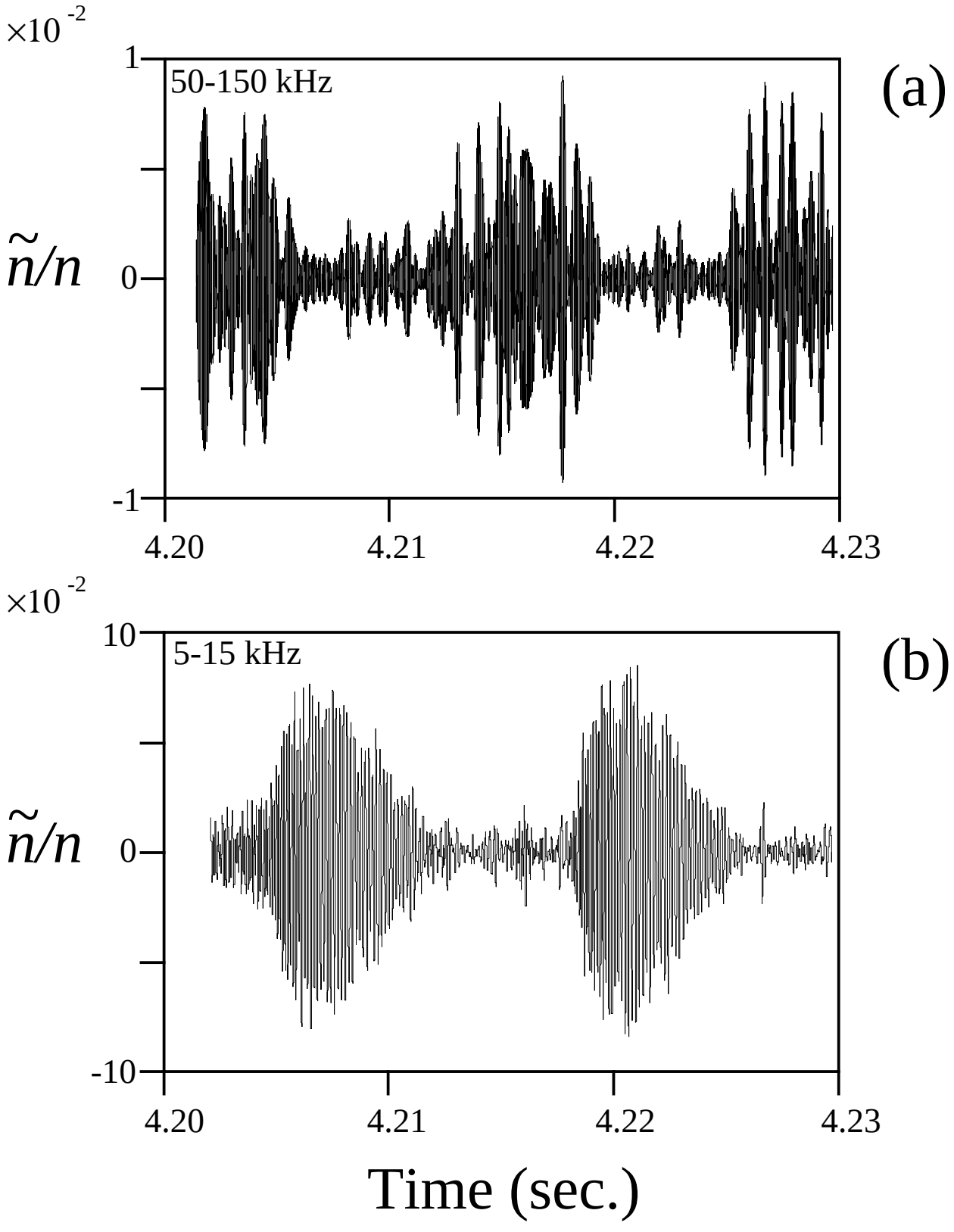
×10 -2
1
50-150 kHz
(a)
ñ/n
0
-1
4.20
4.21
4.22
4.23
×10 -2
10
5-15 kHz
(b)
ñ/n
0
-10
4.20
4.21
4.22
4.23
Time (sec.)

Fig. 6

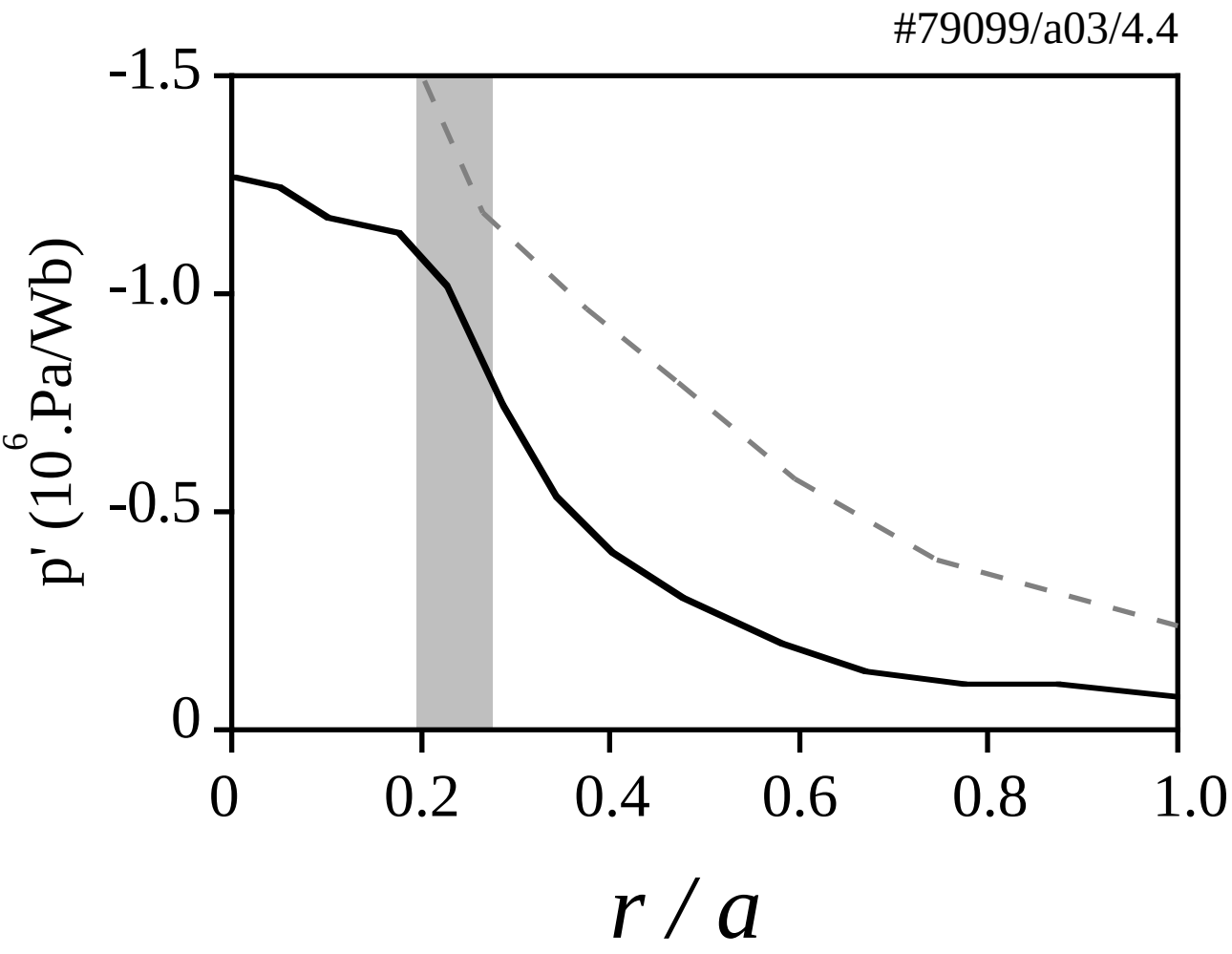

Fig. 7

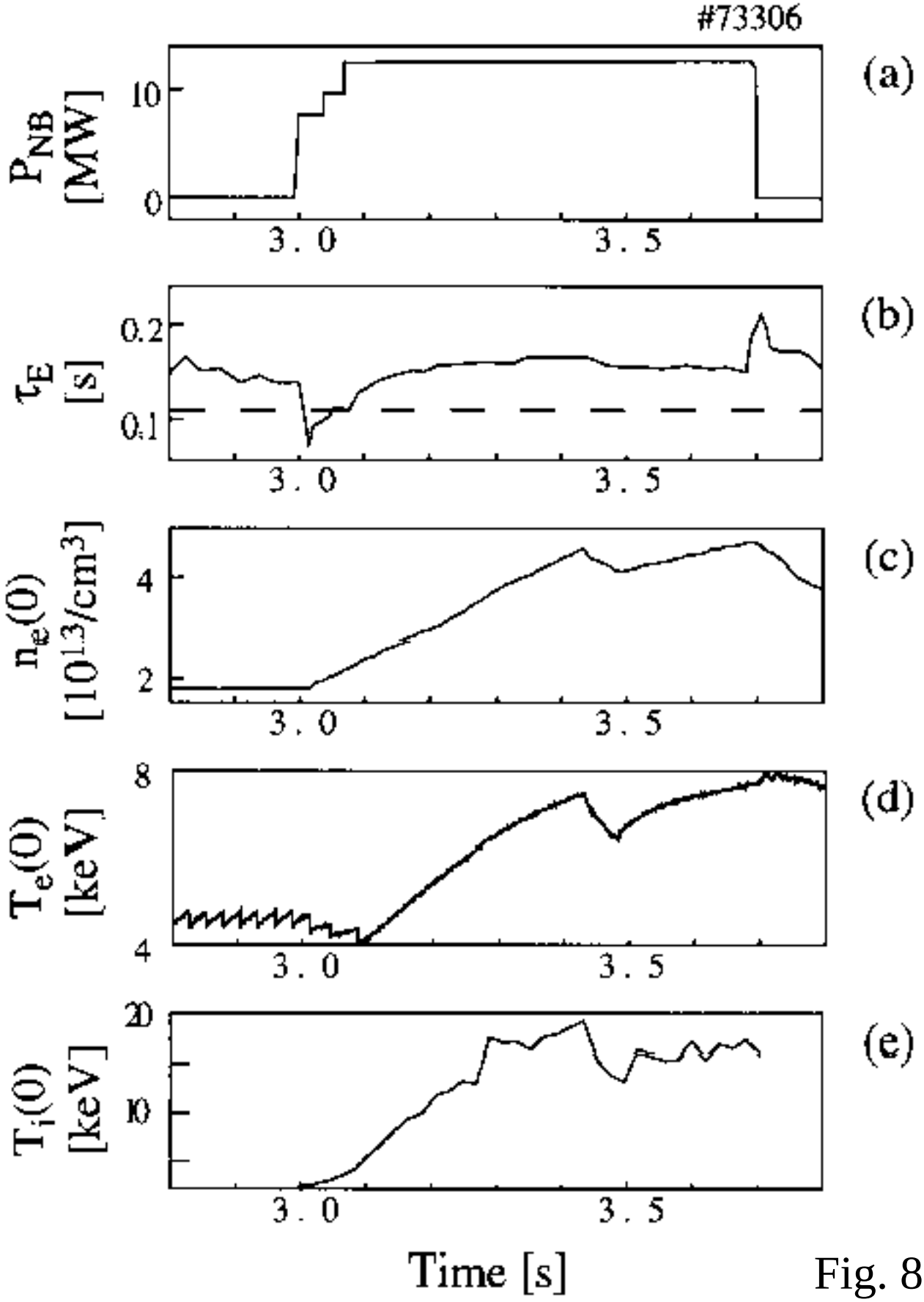
#73306
P_{NB} [MW]
10
0
3.0
3.5
(a)
τ_E [s]
0.2
0.1
3.0
3.5
(b)
$n_e(0)$ [10^{13}/cm^3]
4
2
3.0
3.5
(c)
$T_e(0)$ [keV]
8
4
3.0
3.5
(d)
$T_i(0)$ [keV]
20
10
3.0
3.5
(e)
Time [s]

Fig. 8

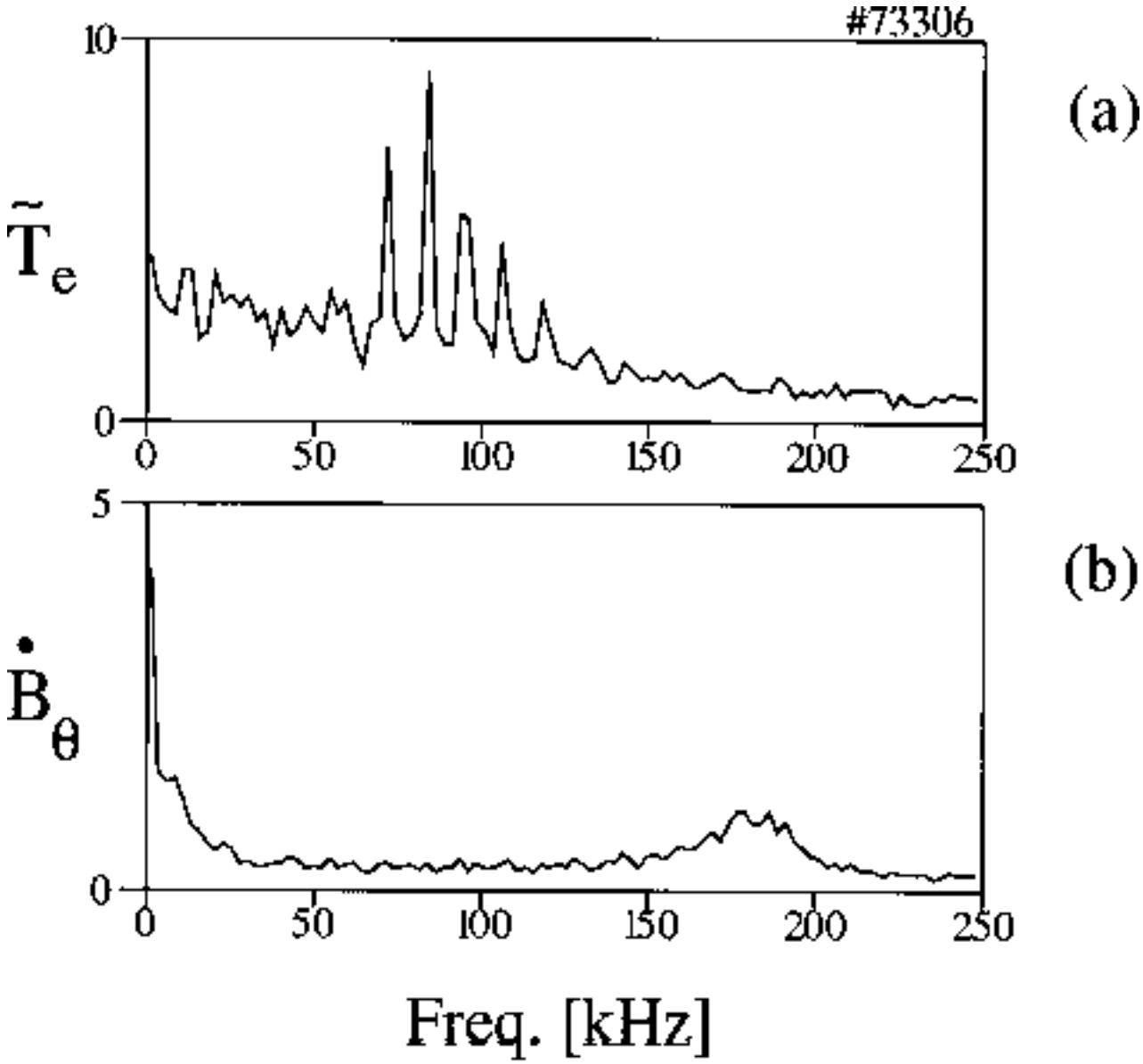
#73306
10
0
$\tilde{T}_e$
(a)
0
50
100
150
200
250
5
0
$\dot{B}_\theta$
(b)
0
50
100
150
200
250
Freq. [kHz]

Fig. 9

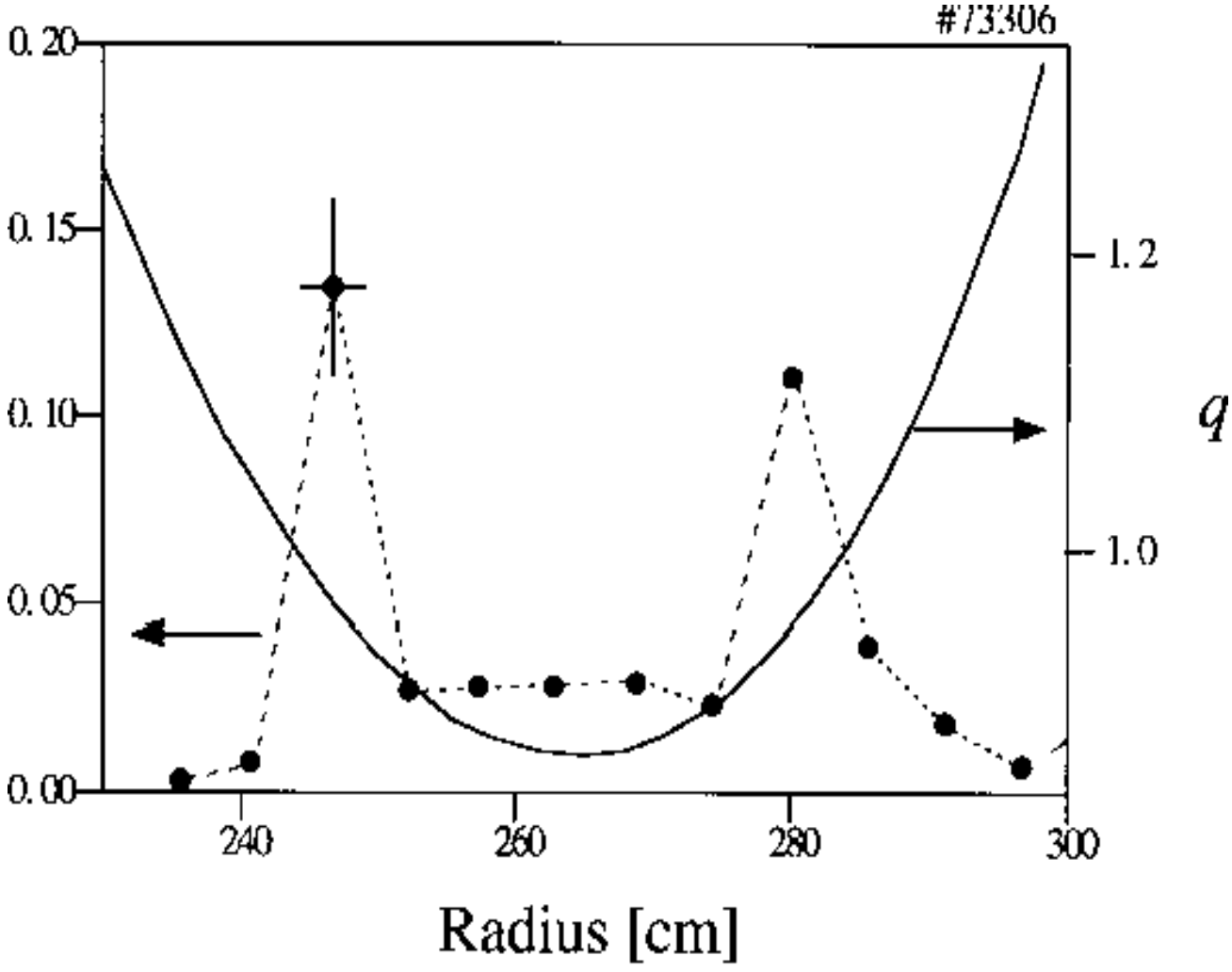

Fig. 10

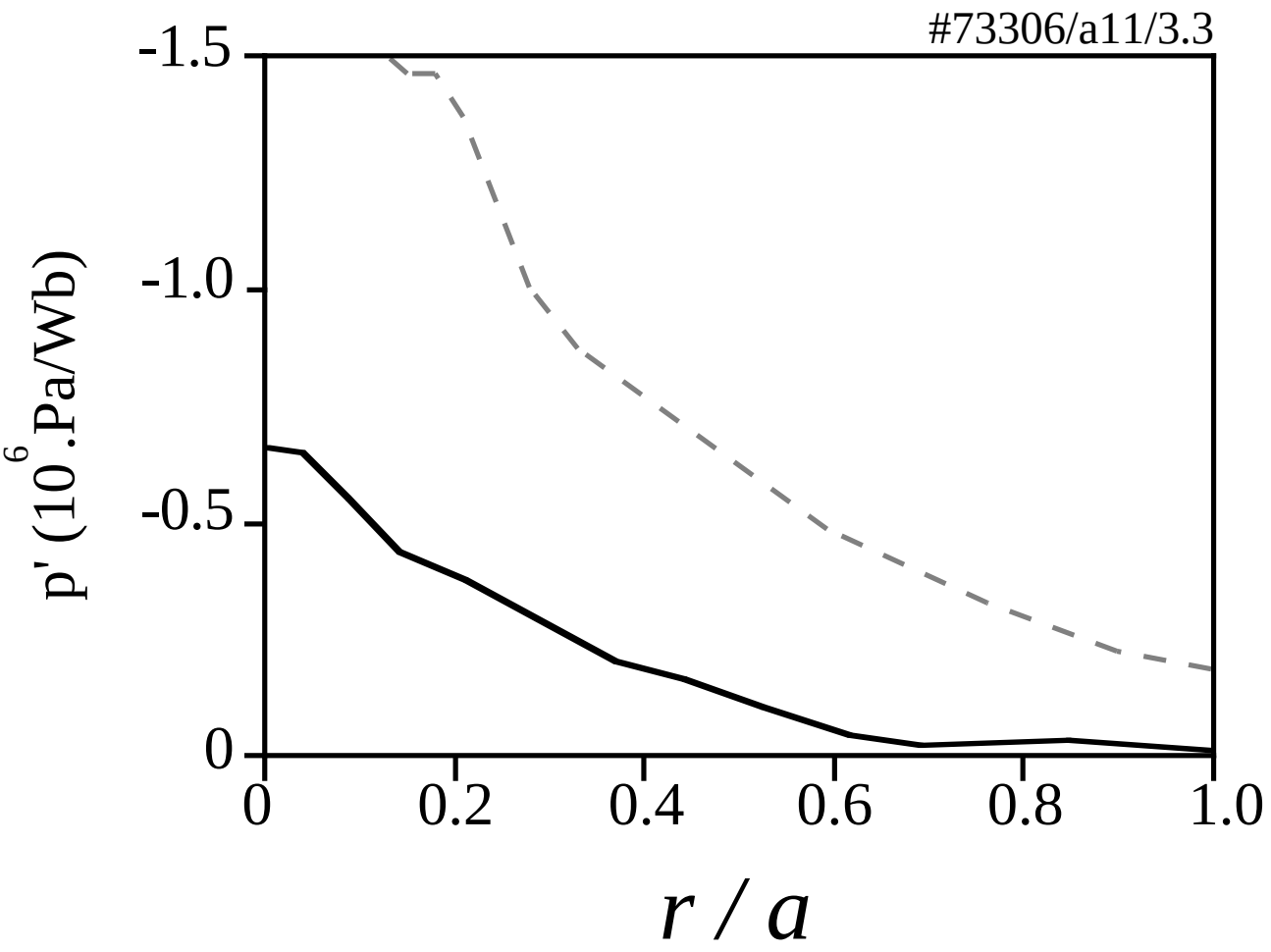

Fig. 11

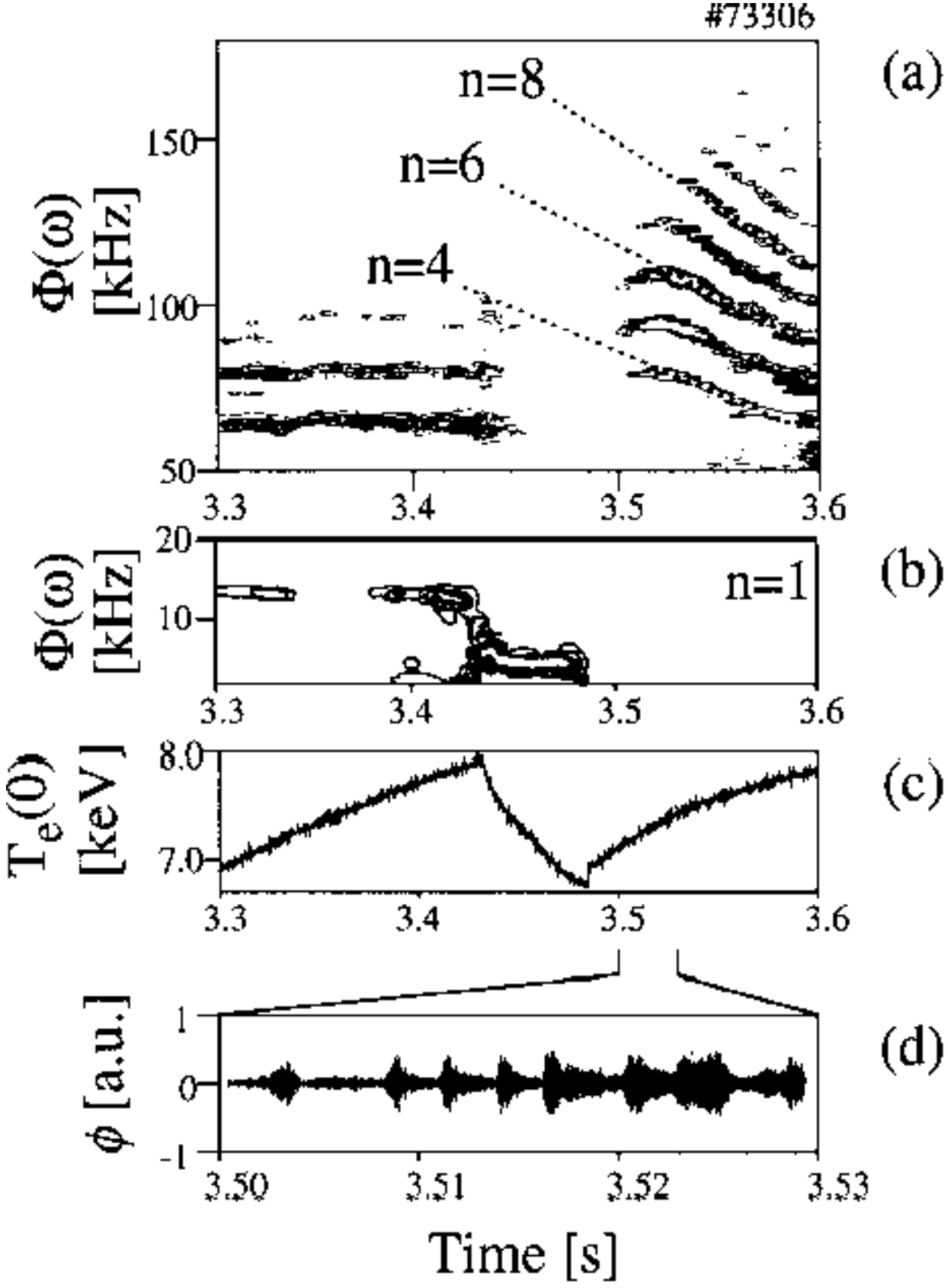
#73306
(a)
n=8
n=6
n=4
Φ(ω) [kHz]
150
100
50
3.3
3.4
3.5
3.6
(b)
n=1
Φ(ω) [kHz]
20
10
(c)
$T_e(0)$ [keV]
8.0
7.0
(d)
φ [a.u.]
1
0
-1
3.50
3.51
3.52
3.53
Time [s]

Fig. 12

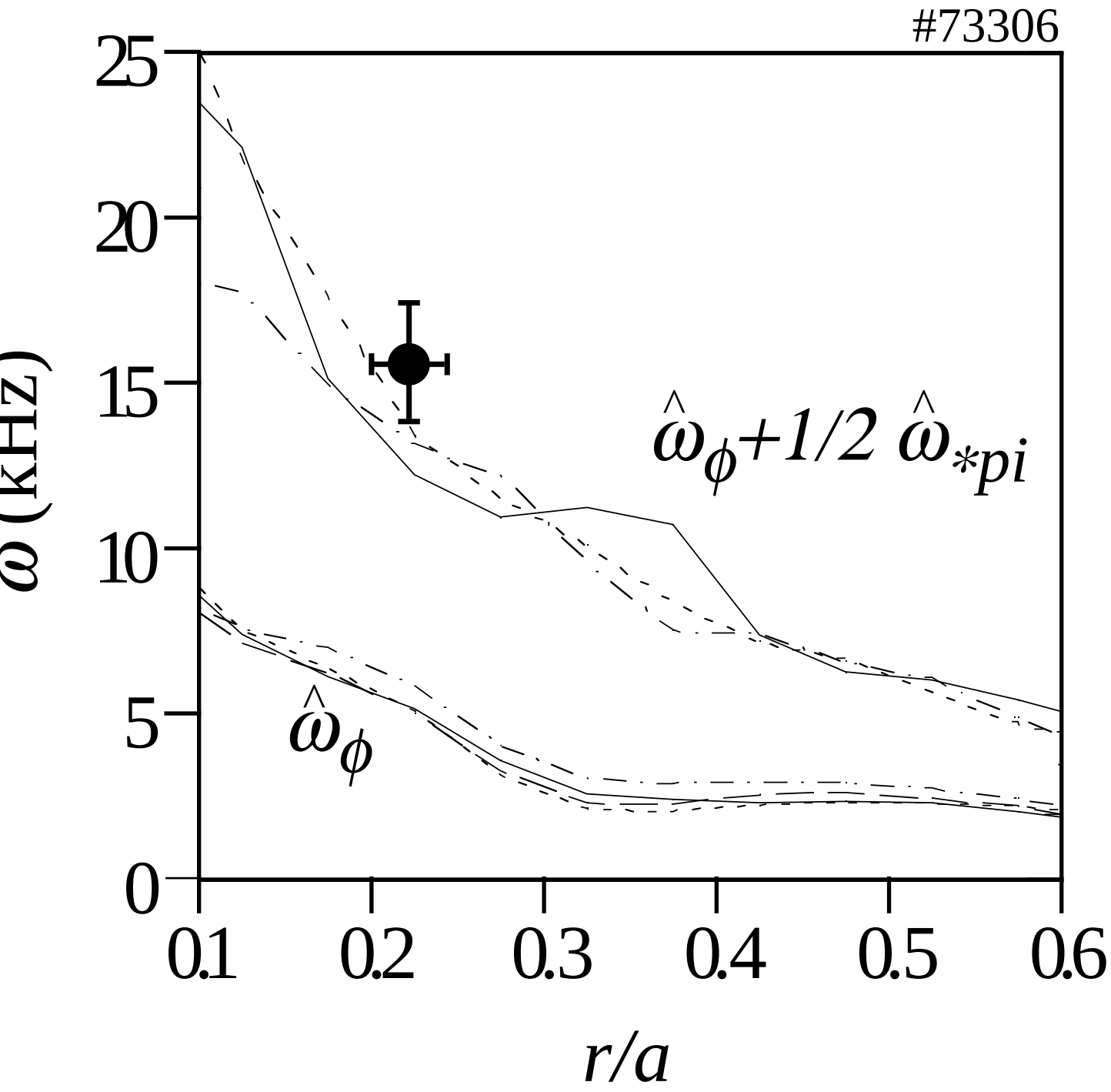
#73306
25
20
15
10
5
0
ω (kHz)
0.1
0.2
0.3
0.4
0.5
0.6
r/a
$\hat{\omega}_\phi$+1/2 $\hat{\omega}_{*pi}$
$\hat{\omega}_\phi$

Fig. 13

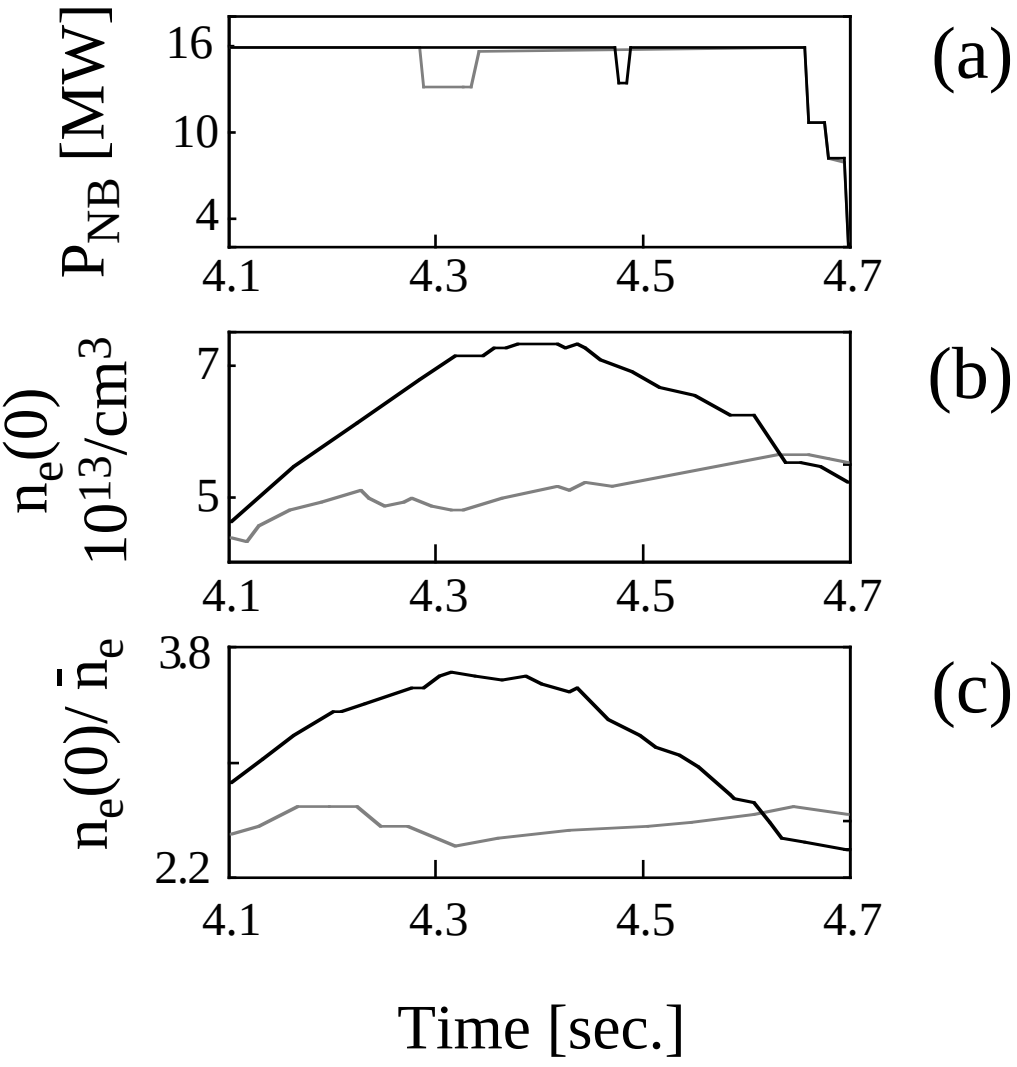
P_{NB} [MW]
16
10
4
(a)
$n_e(0)$ 10^{13}/cm^3
7
5
(b)
$n_e(0)/\bar{n}_e$
3.8
2.2
(c)
4.1
4.3
4.5
4.7
Time [sec.]

Fig. 14

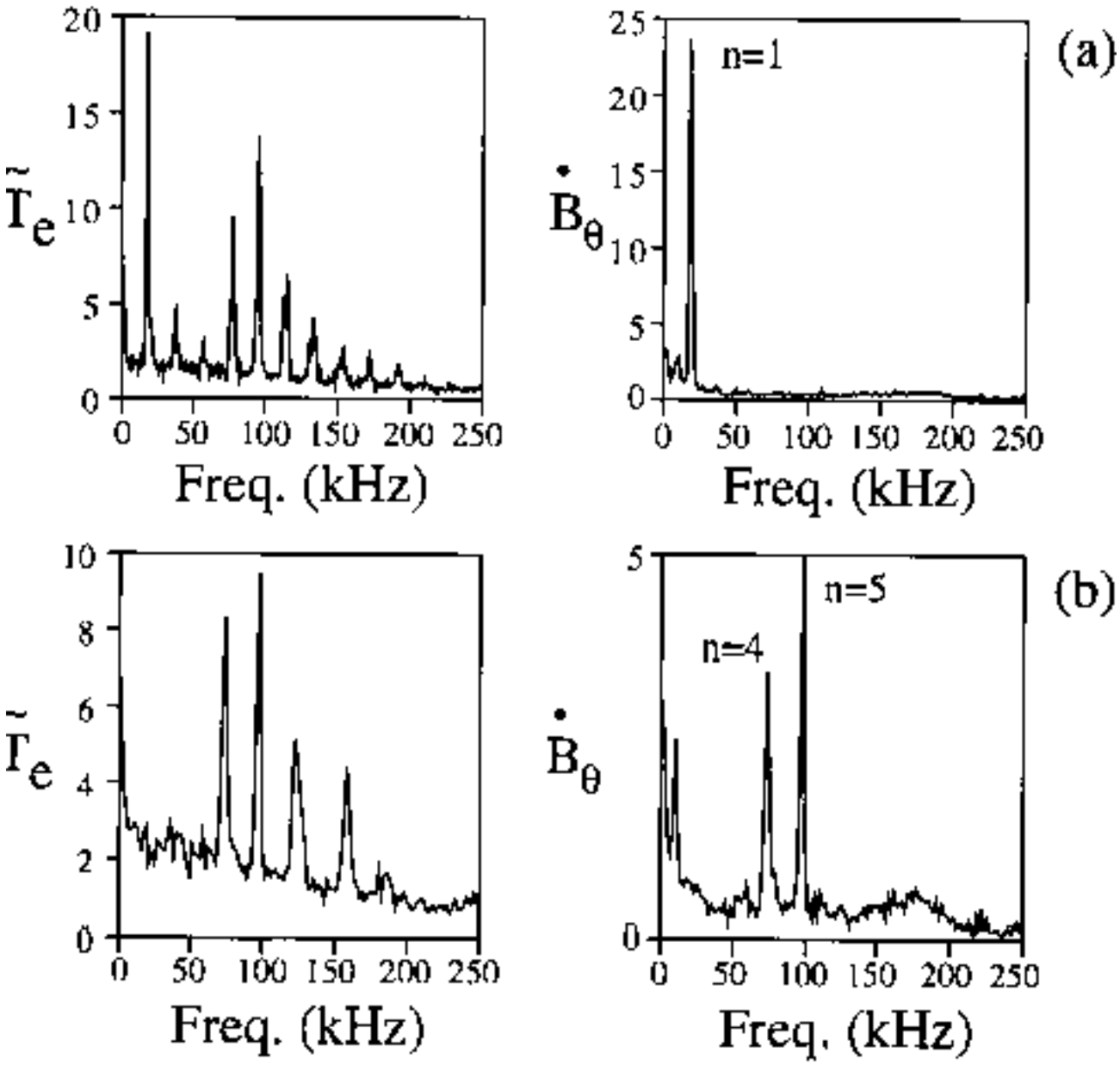
$\tilde{T}_e$
Freq. (kHz)
$\dot{B}_\theta$
n=1
(a)
Freq. (kHz)
$\tilde{T}_e$
Freq. (kHz)
$\dot{B}_\theta$
n=5
n=4
(b)
Freq. (kHz)

Fig. 15

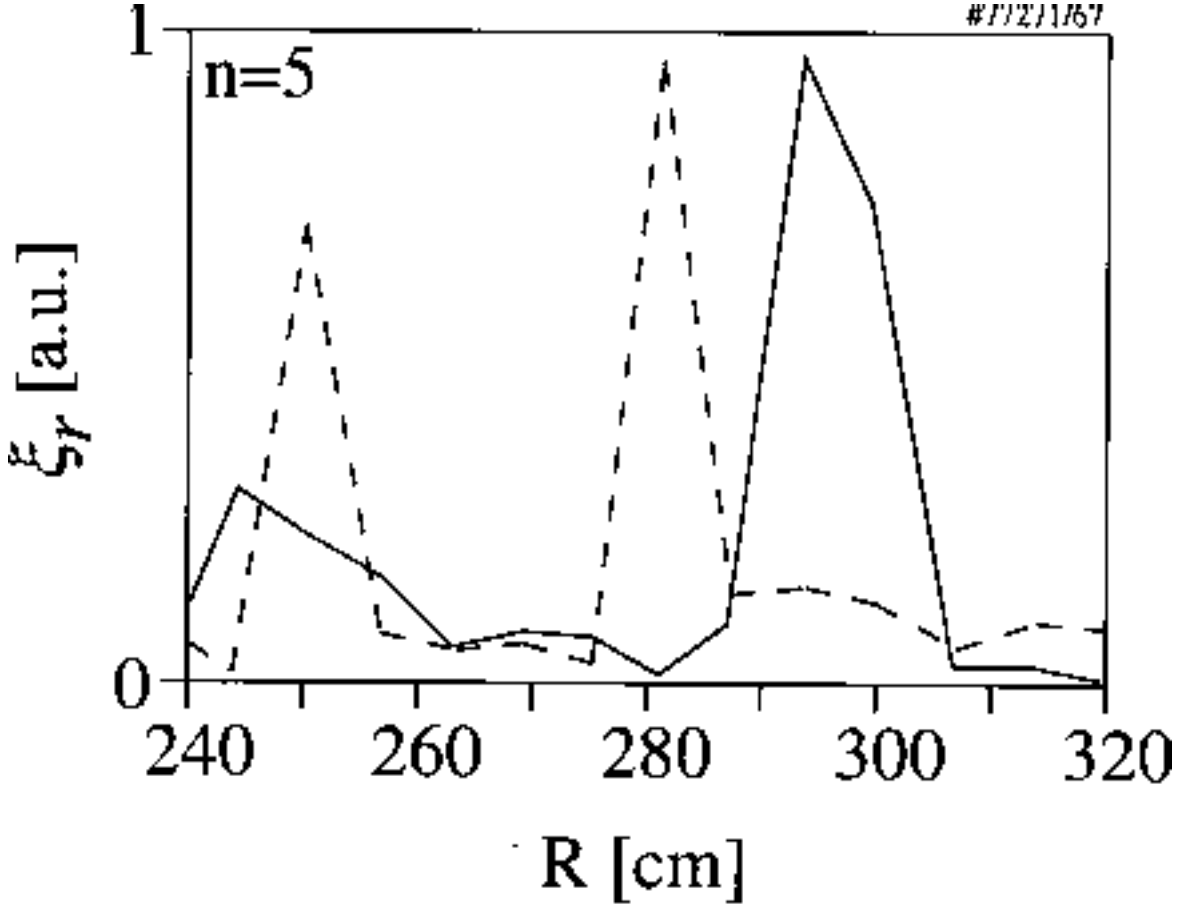

Fig. 16

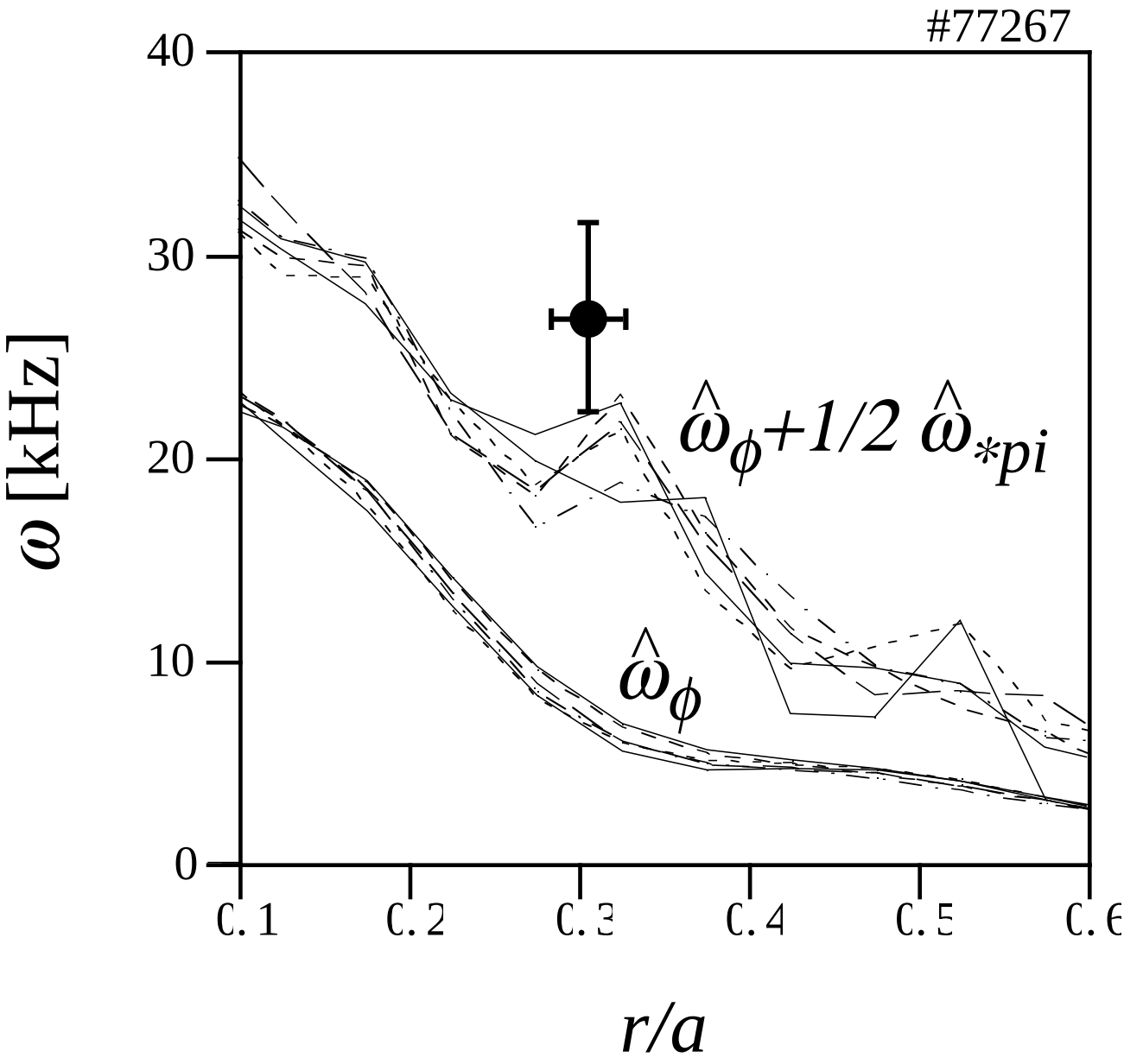
#77267
40
30
20
10
0
ω [kHz]
$\hat{\omega}_\phi$+1/2 $\hat{\omega}_{*pi}$
$\hat{\omega}_\phi$
0.1
0.2
0.3
0.4
0.5
0.6
r/a

Fig. 17

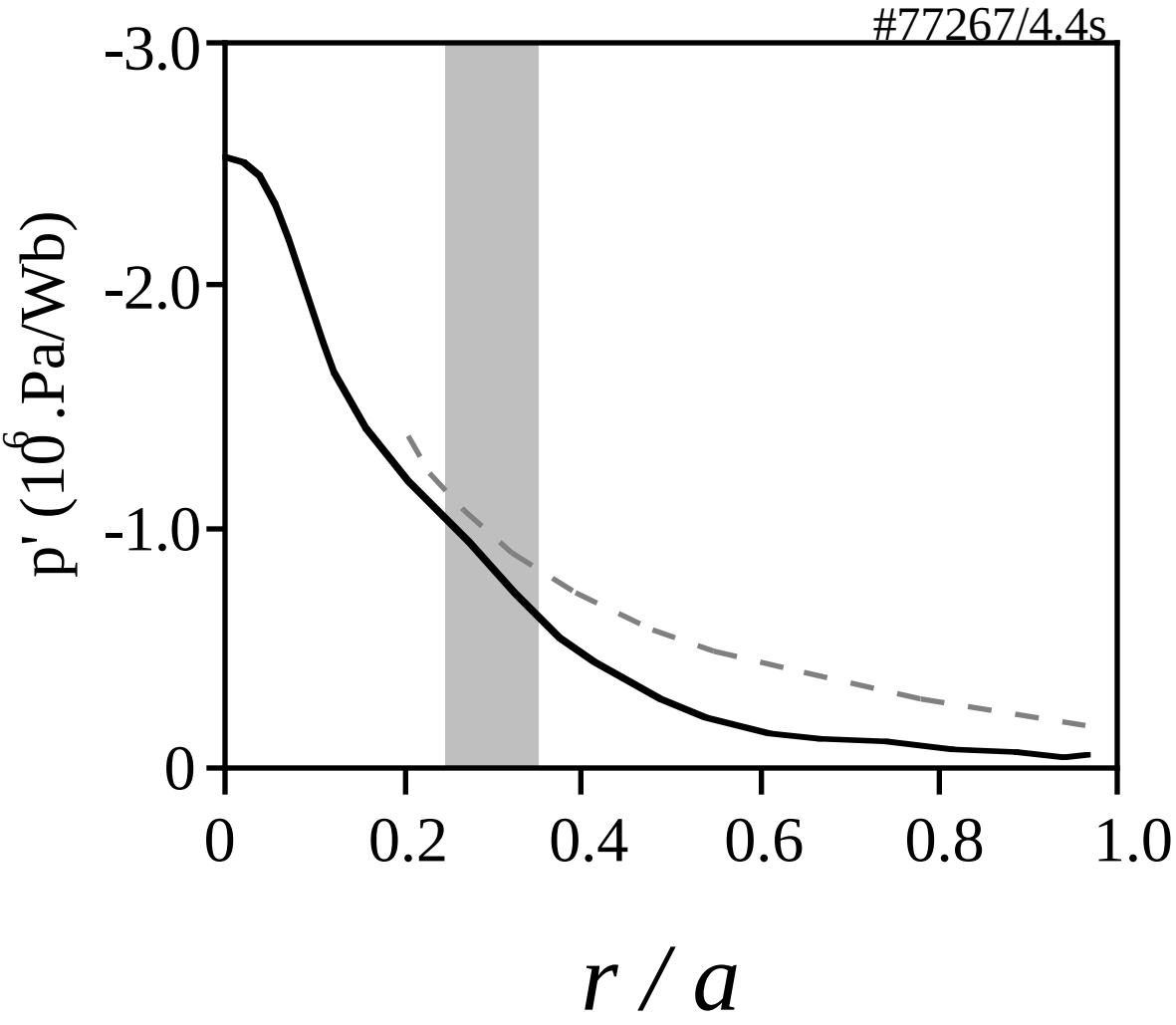

Fig. 18

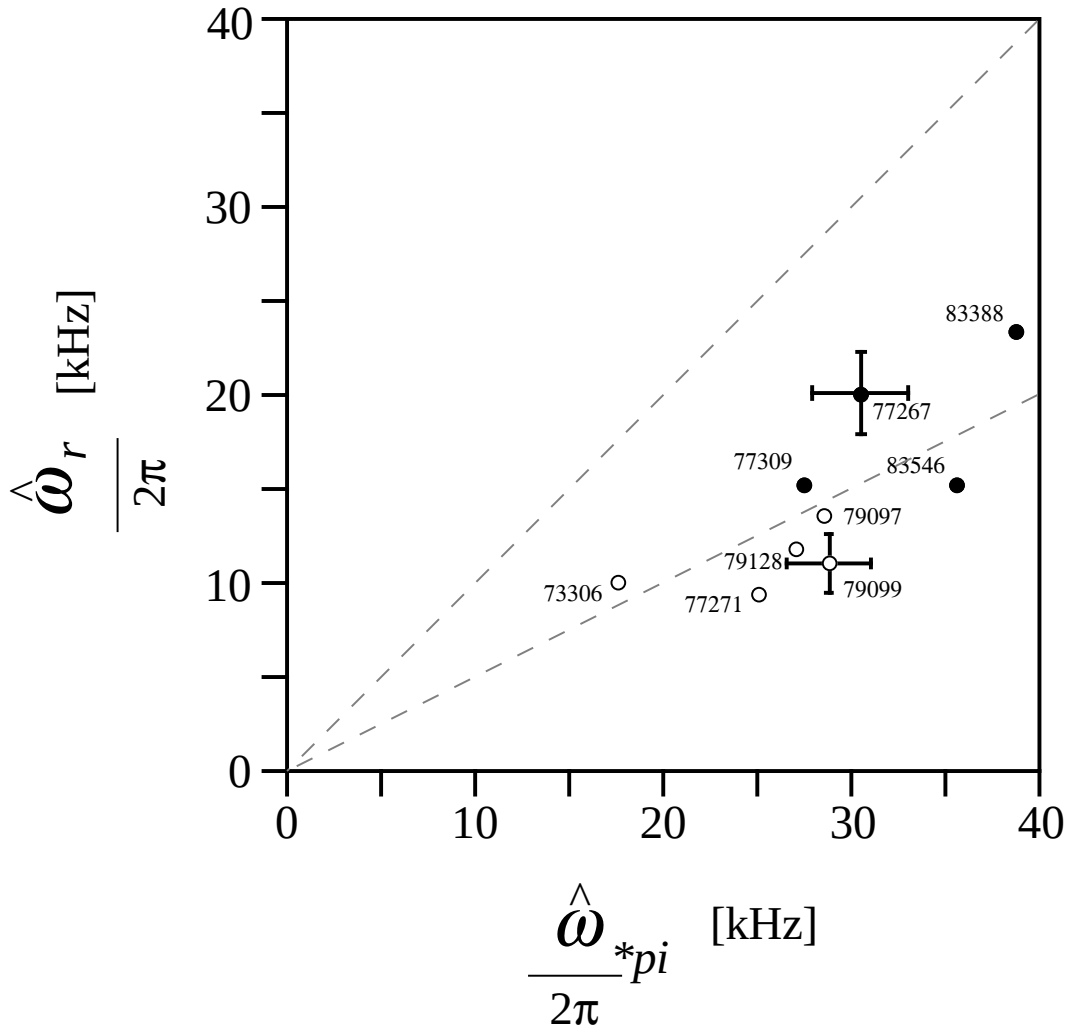
40
30
20
10
0
0
10
20
30
40
$\frac{\hat{\omega}_r}{2\pi}$ [kHz]
$\frac{\hat{\omega}_{*pi}}{2\pi}$ [kHz]
83388
77267
77309
83546
79097
79128
79099
73306
77271

Fig. 19